THE ASTROPHYSICAL JOURNAL, 463:707–725, 1996 June 1

THE CORONAE OF LOW-MASS DWARF STARS

M. S. GIAMPAPA,[1] R. ROSNER,[2] V. KASHYAP,[2] T. A. FLEMING,[3]
J. H. M. M. SCHMITT,[4] AND J. A. BOOKBINDER[5]

Received 1995 February 27; accepted 1995 December 5

ABSTRACT

We report the results of our analysis of pointed X-ray observations of nearby dMe and dM stars using the position sensitive proportional counter (PSPC) on board the *ROSAT* satellite (*Roentgensatellit*). In the cases of those M dwarf stars where PSPC pulse-height distributions of sufficient quality for spectral fitting were obtained, we derive key coronal plasma parameters in order to investigate stellar coronal structure in more detail. In particular, we utilize temperatures and emission measures inferred for one or more distinct components as constraints for the development of semiempirical magnetic loop models as representations of the coronae of low-mass stars. The consistency of these static models as adequate descriptions of the coronae of M dwarfs is then examined.

We find that the coronae of low-mass dwarfs consist of two distinct thermal components: a "soft" component with $T \sim 2$–4×10^6 K and a "hard" component with $T \sim 10^7$ K. We find that the pulse-height spectra are systematically fitted better with "depleted" abundances compared to solar; the high-temperature emission component on dMe stars appears to contribute a systematically larger fraction of the total flux than the corresponding component in dM stars; and the high-temperature emission component on dMe stars is responsible for most of the observed variation in the count rate.

We have modeled the observed temperature components with hydrostatic coronal loop models, and find that: the low-temperature components can be modeled with loops of small size ($l \ll R_*$) and high pressure ($p_0 \gtrsim p_{0\odot}$); and the high-temperature components require solutions with either small filling factors (~ 0.1), large loops ($l \gtrsim R_*$), and high base pressure ($p_0 \gtrsim p_{0\odot}$), or very small filling factors ($\ll 0.1$), small loops ($l \lesssim R_*$), and very high pressure ($p_0 \gg p_{0\odot}$). Based on these observational and model results, we conclude that coronal emission in dMe stars can be interpreted as arising from quiescent active regions (a quiescent, low-temperature component) and compact flaring structures (variable, high-temperature component).

Our conclusion that the coronal geometry for low-mass dwarf stars is dominated by a combination of relatively compact, quiescent loop configurations and an unstable flaring component has implications for both stellar dynamo theory and for our understanding of stellar angular momentum evolution. With regard to rotation in late-type stars, which has a direct bearing on dynamo action, we know from observations that the lowest mass stars spin down (via magnetic braking) more slowly than the more nearly solar-type stars. The compact loops we find for the low-temperature component suggests a natural explanation for the observed mass dependence of angular momentum evolution in late-type, main-sequence stars.

Subject headings: stars: coronae — stars: low-mass, brown dwarfs — X-rays: stars

1. INTRODUCTION

Starting with the *Einstein Observatory*, observations have shown that virtually all late-type stars emit X-rays, indicative of circumstellar (presumably coronal) plasmas at temperatures $\sim 10^6$–10^7 K (e.g., Rosner, Golub, & Vaiana 1985). The origin of coronal emission in main-sequence stars is empirically related to the presence of envelope convection, beginning at a spectral type in the range A7 V–F0 V (Schmitt et al. 1985; Walter 1983), with the actual level of X-ray emission in cool stars related to the stellar rotation rate; this relation is often described by a power-law dependence of the stellar X-ray luminosity on the stellar rotation rate, with a power-law index between one and two (Pallavicini et al. 1981; Fleming, Gioia, & Maccacaro 1989; Hempelmann et al. 1995). However, the precise nature of the heating mechanism in the coronae of the Sun and other late-type stars is unknown. Solar observations suggest that heating processes involve the interaction between convection and magnetic fields at the footpoints of magnetic loops (Tucker 1973; Rosner, Tucker, & Vaiana 1978, hereafter RTV; Rosner et al. 1978; Golub et al. 1980). In addition, more transient activity, from continuous "microflaring" to more classical flaring, may contribute significantly to the total coronal X-ray emission both in the Sun (Parker 1983, 1993) and in cool stars, such as the M dwarf stars (Doyle & Butler 1985; Butler et al. 1986; see Ambruster, Sciortino, & Golub 1987); in the stellar case, however, there has been considerable controversy regarding the weight of the evidence (based largely on temporal X-ray light curves: see Collura, Pasquini, & Schmitt 1988) supporting the detection of microflaring (see Schmitt, Haisch, & Barwig 1993).

A subset of the M dwarfs, namely the dMe flare stars, are especially prodigious sources of X-ray emission, viewed

[1] National Optical Astronomy Observations, National Solar Observatory, P. O. Box 26732, Tuscon, AZ 85726-6732. The National Optical Astronomy Observatories are operated for the National Science Foundation by the Association of Universities for Research in Astronomy.
[2] Department of Astronomy and Astrophysics, University of Chicago, Chicago, IL 60637.
[3] Steward Observatory, University of Arizona, Tucson, AZ 85721.
[4] Max-Planck-Institut für Extraterrestrische Physik, D-8046 Garching bei München, Germany.
[5] Harvard-Smithsonian Center for Astrophysics, Cambridge, MA 01238.

either in terms of their absolute X-ray luminosities, L_X, or in terms of their X-ray emission levels scaled to their bolometric luminosity, L_X/L_{bol} (Fleming et al. 1988, 1993; Schmitt, Fleming, & Giampapa 1995a, hereafter Paper I). The dwarf M stars span a region of the H-R diagram where surface convection does operate, and where magnetic field-related heating mechanisms should be most clearly manifested since the contribution by nonmagnetic (acoustic) heating processes is presumably minimized at these cool photospheric temperatures. These stars are of further interest because irradiation of the underlying atmosphere by the overlying corona may be the source of *chromospheric* heating in these objects (Cram 1982).

Most models for stellar dynamos would predict a fundamental change in the principal mechanism for the generation of interior magnetic fields at the point where stellar interiors become fully convective (e.g., Rosner & Vaiana 1980; Giampapa & Liebert 1986; Rosner & Weiss 1992) and by implication, a change in coronal activity (given the underlying assumption that stellar magnetic fields are largely responsible for stellar activity). Moreover, some theories of coronal heating suggest that the coupling efficiency between the convection zone and magnetic loops changes significantly along the lower main sequence (e.g., Mullan 1984). Thus, observations of X-ray emission from stars along the lower main sequence can potentially provide a number of constraints on models for both stellar magnetic field production and the mechanism(s) for coronal heating. Finally, we note that because of the sheer number of M dwarfs in the Galaxy, these stars could make a significant contribution to the diffuse X-ray background (Rosner et al. 1981; Schmitt & Snowden 1990; Kashyap et al. 1994).

In view of the importance of these objects as observational probes for dynamo theory and theories of coronal heating, as well as their potential role in the galactic environment, we implemented a program of pointed *ROSAT* PSPC observations of selected M dwarfs in order to address specific issues. Our results for both the level of X-ray emission (L_X) and the "efficiency" of coronal heating (as measured by the parameter L_X/L_{bol}) in the coolest dMe stars thus far observed with *ROSAT* have already been summarized by Fleming et al. (1993). In particular, these investigators do not find evidence for a turnover in coronal heating efficiency. More specifically, the distribution function for L_X/L_{bol} is independent of spectral type at the coolest end of the main sequence observed by *ROSAT*. We extend these investigations in this paper to selected *quiescent* dM (i.e., non-dMe) stars that were not detected by *Einstein* and the *ROSAT* all-sky survey (RASS). Among the questions that we address is whether plasma at coronal temperatures is at all present in these less active stars, i.e., whether coronae eventually vanish in the kinematically older, low-mass dwarfs. In the cases of those dMe and dM stars where PSPC pulse-height distributions of sufficient quality for spectral fitting were obtained, we derive key coronal plasma parameters in order to investigate stellar coronal structure in more detail. In particular, we utilize temperatures and emission measures inferred for one or more distinct components as constraints for the development of semiempirical magnetic loop models as representations of the coronae of low-mass stars. The consistency of these static models as adequate descriptions of the coronae of M dwarfs is then examined.

We discuss the observational approach and the data reduction methods in § 2. The results from the spectral fitting are described in § 3, and discussion of our loop atmosphere modeling of our spectroscopic data is found in § 4. We summarize our principal findings and delineate directions for future research in § 5.

2. OBSERVATIONS

2.1. *Optical Data*

The program objects, along with adopted stellar parameters that are relevant to this investigation, are listed in Table 1. The spectral types for the program objects are from either Kirkpatrick, Henry, & McCarthy (1991) or Boeshaar (1976). The distances are derived from the parallax measurements which are compiled in the Third Catalogue of Nearby Stars (preliminary version; Gliese & Jahreiss 1991). Stellar radii are taken from Reid & Gilmore (1984), while bolometric luminosities were calculated from the absolute K magnitude using the relation of Veeder (1974). We utilize the mass-luminosity relations determined by Henry & McCarthy (1993) for low-mass stars, and colors from Veeder (1974), to estimate masses for the M dwarfs in Table 1. These mass estimates are used, along with the radii, to estimate the stellar surface gravity; these computed surface gravities are then used to calculate characteristic coronal scale heights as part of our loop model analysis. Other sources of basic data for individual objects in Table 1 include Fleming et al. (1993, VB 8), Liebert, Boroson, & Giampapa (1984, LHS 2924), Mullan, Stencel, & Backman (1989, GL 754), Linsky et al. (1982, AD Leo), and Bessell (1990).

TABLE 1

ADOPTED STELLAR PARAMETERS

Star	Spectral Type[a]	Kinematic Population	d (pc)	$R_*/R_\odot$	$M_*/M_\odot$	log g (cgs)
GL 388 (AD Leo)	M3.5 Ve	YD	4.90	0.49	0.44	4.70
GL 644A (Wolf 630)	M4 Ve	OD	6.50	0.678	0.45	4.43
GL 406 (CN Leo)	M6 Ve	OD	2.39	0.15	0.10	5.08
LHS 292	M6.5 Ve	OD	4.52	...	...	...
GL 644C (VB 8)	M7 Ve	OD	6.50	0.103	0.082	5.32
GL 752B (VB 10)	M8 Ve	OD	5.66	...	...	...
LHS 2924	M9 e	OD	11.0	...	...	...
GL 411	M2 V	OD	2.52	0.374	0.39	4.88
GL 699 (Barnard's star)	M4 V	Halo	1.83	0.182	0.144	5.07
GL 754	M4 V	OD	5.69	...	...	...
GL 299	M4 V	Halo	6.76	...	...	...

[a] The "e" designation indicates the presence of Hα emission.

TABLE 2

ROSAT PSPC POINTED OBSERVATIONS OF M DWARFS

Star	d (pc)	Exposure (ks)	Count Rate (counts s^{-1})	f_X [a]	log L_X [b]	log (L_X/L_{bol})
GL 388 (AD Leo)	4.90	15.242	3.6709 ± 0.0041	2.90	28.92	−3.068
GL 644A (Wolf 630)	6.41	8.780	3.0160 ± 0.0067	1.12	28.75	−3.198
GL 406 (CN Leo)	2.35	1.4930	1.0293 ± 0.0268	0.872	27.78	−2.856
LHS 292	4.52	5.300	0.0085 ± 0.0015	0.00386	25.98	−4.433
GL 644C (VB 8)	6.41	8.780	0.0865 ± 0.0032	0.0683	27.54	−2.838
GL 752B (VB 10)	5.92	7.280	$<2.9 \times 10^{-3}$	$<1.6 \times 10^{-3}$	<25.78	<−4.473
LHS 2924	11.0	25.029	$<5.4 \times 10^{-4}$	$<3.8 \times 10^{-4}$	<25.74	<−4.268
GL 411	2.52	10.389	0.1823 ± 0.0043	0.0904	26.84	−5.064
GL 699 (Barnard's star)	1.79	4.515	0.0254 ± 0.0026	0.00942	25.58	−5.498
GL 754	5.71	6.964	0.0047 ± 0.0011	0.00141	25.74	−5.534
GL 299	6.62	7.359	$<1.2 \times 10^{-3}$	$<6.48 \times 10^{-4}$	<25.55	<−5.394

[a] Observed flux (f_X) is in units of 10^{-11} ergs s^{-1} cm^{-2}.
[b] Luminosity $L_X = 4\pi d^2 f_X$ is in units of ergs s^{-1}.

2.2. *X-Ray Data*

We utilized the *Röntgensatellit* (*ROSAT*; Trümper 1983) in conjunction with the position sensitive proportional counter (PSPC) to obtain pointed X-ray observations of selected dwarf M stars in the photon energy range 0.1–2.4 keV.

We began our data analysis by employing a maximum likelihood (ML) algorithm fixed at the optical position of each star in the sample in order to determine if it had been detected or not.[6] The ML algorithm was also used to calculate the total PSPC count rate of the source above the background, or upper limit thereof. A more detailed description of our PSPC analysis techniques can be found in Fleming et al. (1993). The PSPC count rates were converted into X-ray flux using the hardness ratio-dependent conversion factors given by Fleming et al. (1995a). The observed count rates and errors, the corresponding observed fluxes at Earth, the inferred X-ray luminosities, and the ratios of the X-ray luminosity to the bolometric luminosity, or 95% confidence upper limits to these quantities in the cases of non detections, are given in Table 2.

[6] We have correctly taken the (large) proper motions of these stars into account while identifying the detected X-ray sources.

3. X-RAY ANALYSIS

3.1. *Spectral Analysis*

In those cases for which the total counts were sufficient, we fit Raymond-Smith (RS) plasma models to the PSPC pulse-height distributions, using the XSPEC package (v.8.4 unless otherwise specified). The results of these fits, which are based on a minimization of the χ^2 statistic, are presented in Table 3. We display illustrative spectral fits for dMe and dM stars in Figure 1. The sharp contrast between the spectra in the high-energy channels is clearly evident.

Because there are no accurate metallicity measurements for these red dwarfs, we initially adopted solar values for metal abundances during spectral analysis. The results of then fitting two-temperature (2-T) RS thermal spectra to the data are shown in Table 3. Now the assumption of solar metal abundances is clearly inappropriate for stars such as

TABLE 3

SPECTRAL ANALYSIS RESULTS

Star	Metals ($Z_\odot = 1$)	N_H (10^{19} cm^{-2})	T_L (10^6 K)	EM_L (10^{11} cm^{-5})	T_H (10^6 K)	EM_H (10^{11} cm^{-5})	χ^2/d.o.f.
	1	7.38	1.61	4.18	10.03	3.47	168/21
GL 388 (AD Leo)	0.1	2.6	3.5	12.9	8.9	24.6	24/20
	(0.07–0.13)	[2.1–3.3]	[2.4–4.69]	[10.2–17.6]	[8.4–9.8]	[19.6–27.4]	
	1	2.3	1.86	5.2	9.7	3.7	40/21
GL 644A (Wolf 630)	0.29	2.8	1.97	12.5	9.12	9.79	25/21
	(0.27–0.41)	[1.9–3.7]	[1.87–2.13]	[11.7–13.5]	[8.86–9.45]	[9.5–10.1]	
	1	0.01	1.71	0.85	8.23	2.03	26/16
GL 406 (CN Leo)	(0.2–5)	[0–32]	[0–2.09]	[0.65–0.89]	[7.43–8.94]	[1.9–2.2]	
	1	1.93	1.61	0.12	9.91	0.15	8.2/20
GL 644C (VB 8)	0.2	1.6	1.50	0.21	8.71	0.63	6.9/20
	(0.05–5)	[0–23.9]	[0–2.26]	[0.08–2.6]	[7.61–10.6]	[0.5–0.73]	
	1	5.95	1.24	0.52	7.53	0.08	10.5/12
GL 411	0.3	3.05	1.30	1.24	6.68	0.32	10/12
	(0.03–5)	[0–19]	[0–1.57]	[0.92–4.8]	[4.86–8.29]	[0.26–0.45]	
	1	0	1.81	0.052	...	...	12.3/14
GL 699 (Barnard's star)	0.08	0.01	2.30	0.325	...	...	12/14
	(0–5)	[0–11]	[0–3.35]	[0.26–0.82]			

NOTES.—(1) Spectral fits were carried out with five free parameters, holding the abundance fixed at the "best-fit" value. The numbers within brackets denote 90% confidence limits on the fit parameters. (2) The range of abundances that give adequate spectral fits ($\Delta\chi^2 < 2.7$ from the best-fit) are shown within parenthesis. (3) In some cases, the parameters are not constrained (e.g., T_L for VB 8). This is a consequence of the characteristic spectral response of the *ROSAT* PSPC.

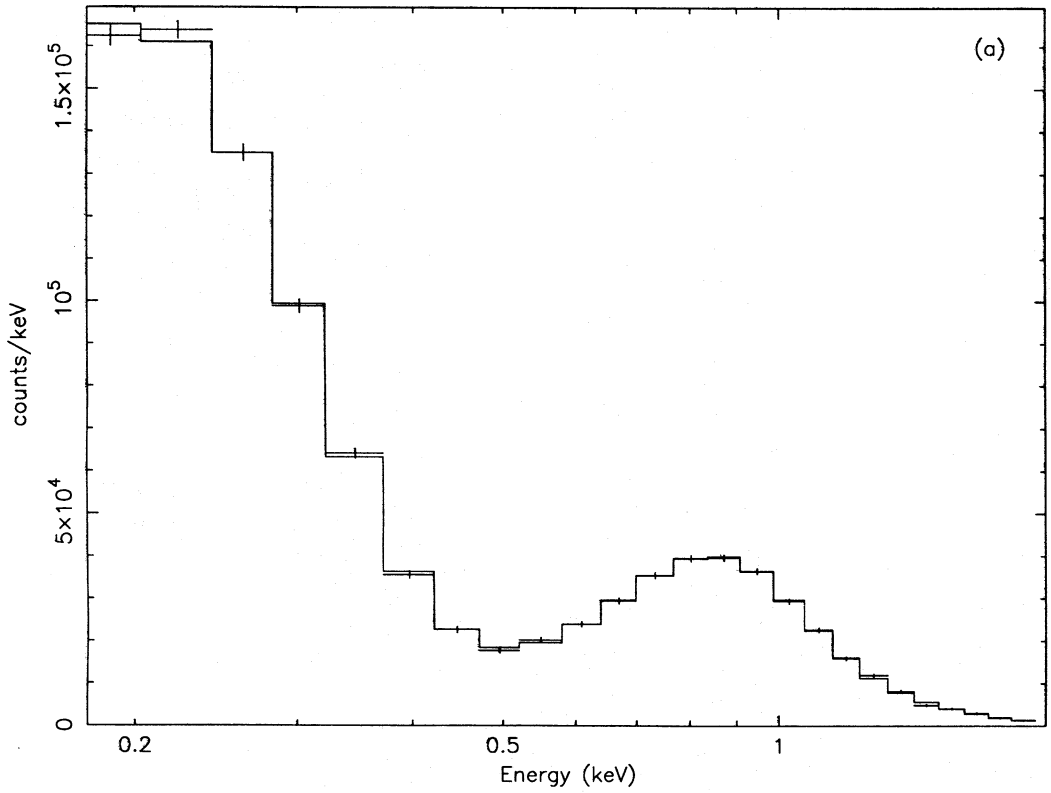

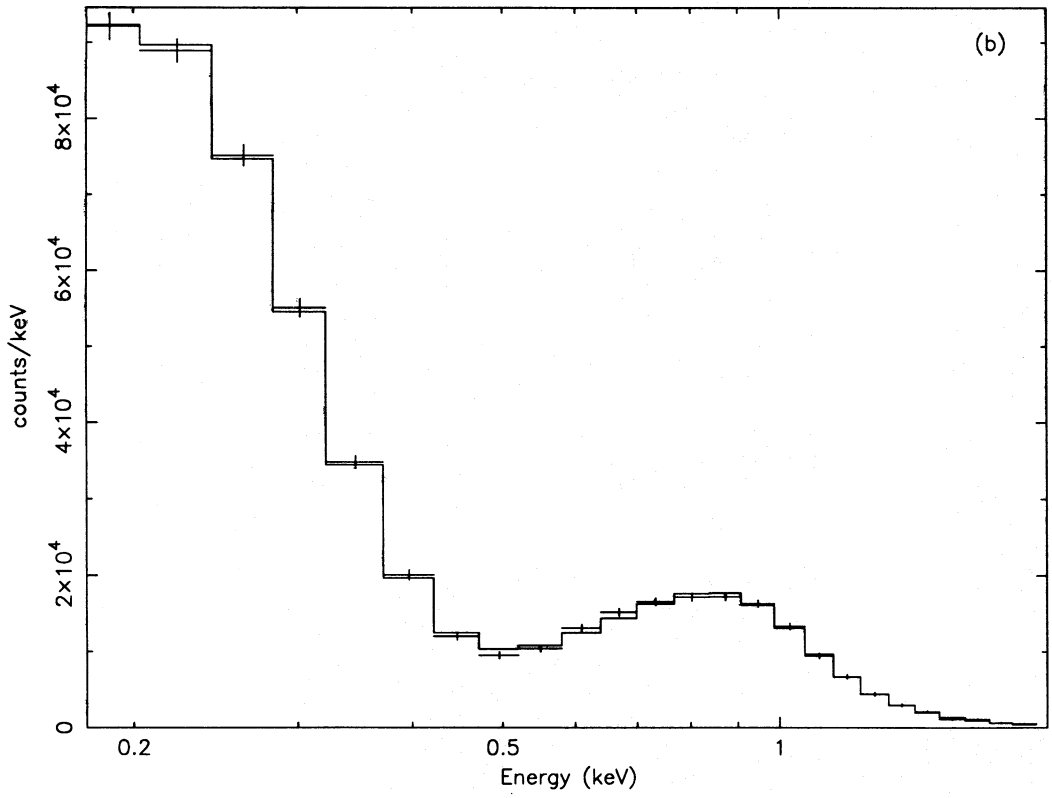

FIG. 1.—X-ray spectra of three representative stars in our sample. (*a*) The dMe star AD Leo; (*b*) the dMe star Wolf 630; (*c*) the dM star GL 411.

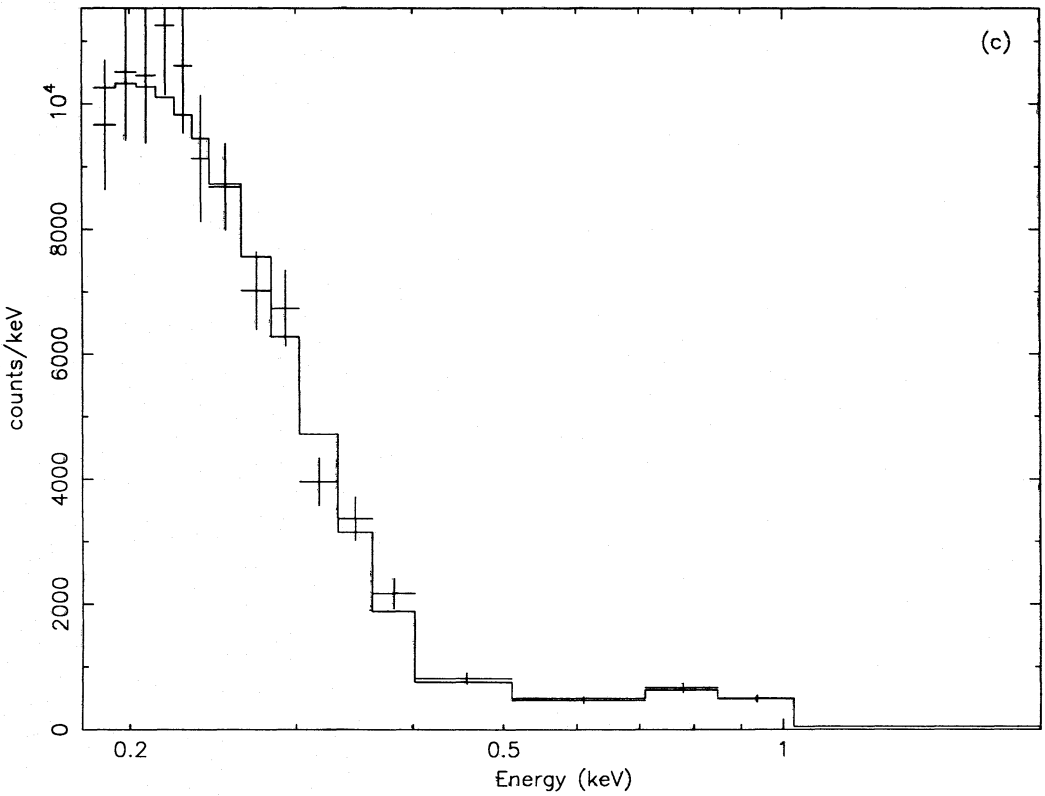

FIG. 1—*Continued*

GL 699 (Barnard's star) and GL 411. We therefore explored the effects of varying metal abundances (Z) by fitting 2-T thermal spectra (with five free parameters: column density to source N_H, two temperature components T_L and T_H, and the corresponding emission measures EM_L and EM_H; the adopted Z was held constant) over a wide range of values for Z. In this manner, we are able to determine the value of Z for which the observed spectrum was fitted best; these values and the corresponding fit parameters are also reported in Table 3. These results are *not* to be interpreted as a measurement of abundances in the coronae of these stars: the relatively poor spectral resolution of the PSPC, combined with uncertainties in atomic parameters and the expected model dependence of the results preclude such a conclusion. However, our results are consistent with independent measurements with *ASCA* and *EUVE* that consistently find that coronal abundances are systematically lower than solar abundances (Singh et al. 1995, and references therein; Stern et al. 1995b; Schmitt et al. 1995b); note that Schmitt et al. (1995b) point out that lower resolution X-ray measurements face difficulties in disentangling emission measure distribution and abundance effects and tend to have a bias toward lower abundances.

We further note that even if the metallicity is known from, say, analysis of photospheric spectra, the example of the solar corona cautions that the relative distribution of metal abundances in the corona may be the same as that in the photosphere (FIP effect; see, e.g., Meyer 1985); in the *EUVE* spectrum of α Cen evidence for the FIP effect has been found (see Drake et al. 1995b), while in contrast, an analysis of the EUV spectrum of Procyon (F5 IV) indicates no differences between the elemental abundances in the corona and photosphere of this nearby active star (Drake et al. 1995a, c). In any case, based on our fits to the X-ray data, we find indications of much lower metallicity Z than solar; this result is however statistically significant only for the two brightest stars in our sample (AD Leo with $0.075 < Z < 0.13$ and Wolf 630 with $0.27 < Z < 0.41$).

Because the above-described abundance analysis is far from definitive, and because the preponderance of the evidence is that there are real departures from the solar metallicity value ($Z = 1$), it is important to establish the resulting impact on our results and interpretations. For this reason, we have carried out a sensitivity analysis which shows that the primary effect of uncertain metal abundances is on the derived emission measures. In particular, the emission measures can increase by an order of magnitude when metals are deficient (see Table 3). Our principal conclusions however do not depend on the magnitudes of the emission measures and are therefore not altered despite the uncertainties in this aspect of the analysis.

Recalling our results from Papers I and II, (Fleming, Schmitt, & Giampapa 1995b [Paper II]), we find that dMe stars are characterized by a X-ray luminosity function with a substantial range, e.g., $L_X \sim 10^{26}$–10^{29} ergs s^{-1}; we also find that for these stars, $L_X/L_{bol} \sim 10^{-4}$. In contrast, the X-ray luminosity function for dM stars is largely confined to $L_X \leq 10^{27}$ ergs s^{-1}; and furthermore, $L_X/L_{bol} \sim 10^{-7}$ to 10^{-6}. To compare, the quiet solar corona emits $L_X \simeq 2 \times 10^{27}$ ergs s^{-1}, corresponding to $L_X/L_{bol} \simeq 5 \times 10^{-7}$ (see Vaiana & Rosner 1978). Thus, the coronal heating "efficiency" (as measured by the X-ray to bolometric luminosity ratio) is 2–3 orders of magnitude smaller for dM stars than for active dMe stars. However, even in the quiescent M dwarfs, this quantity can be greater than the value for the Sun.

One important issue is whether there are late-type dwarf stars with no coronae. This question arose first in the

context of GL 411, a nearby M2 dwarf whose far-UV spectrum is dominated by chromospheric emission lines from neutral metal species, but which does not exhibit high-temperature ($\sim 10^5$ K) emission lines characteristic of transition region plasmas, such as the C IV λ1549 blend as seen in *IUE* low-dispersion spectra (Linsky et al. 1982). There is no reported *Einstein* observation of this quiescent M dwarf. However, Schmitt & Rosso (1988) report an X-ray detection of GL 411 with *EXOSAT*.

Our detection of X-ray emission in GL 411, using PSPC pointed observations, confirms the existence of a corona, even in this kinematically older object.[7] An inspection of the RASS data reveals that GL 411 was indeed detected in the sky survey. We note that Schmitt & Rosso (1988) detected with *EXOSAT* all the targets in their small sample (seven stars) of nearby ($d < 6$ pc) M dwarfs, with the exception of GL 754 (dM7). However, we also detect this object in our pointed *ROSAT* PSPC data (Table 2). This result, along with that for GL 411, offers further evidence for the suggestion that all M dwarfs are coronal X-ray sources. The findings from the RASS support this hypothesis (Fleming, Schmitt & Giampapa 1995b; Paper II).

All the detected stars in our sample except the faintest one (GL 699) require two-temperature fits, with the temperatures being typically a few times 10^6 K and $\sim 10^7$ K, respectively. We recall that in previous investigations, based on *Einstein Observatory* data, Swank & Johnson (1982) and Schmitt et al. (1990) found evidence for high-temperature plasma in conjunction with low-temperature gas in M dwarfs. This is typical of other coronal sources, such as RS CVn systems (Swank et al. 1981; Schmitt et al. 1990). By contrast, however, Schmitt et al. (1990) reported that main sequence F and G stars did not exhibit a high-temperature component, or it was very weak, as seen in their *Einstein* IPC data.

We also find that the corresponding two emission measure components are comparable in magnitude for dMe stars, while the emission measure of the hard component is much less than that of the soft component in dM stars. Thus, we find that in addition to the obvious evolutionary decline in both L_X and L_X/L_{bol} between dMe and the quiescent dM stars, the contribution of the hard component relative to the soft component also decreases (see also Fleming et al. 1995b).

A remaining question is whether coronal temperatures depend on stellar age; this question is raised (but not answered) by our result that the temperature of the hard component for GL 411 is significantly lower than that for the dMe stars. It is very difficult (and most likely impossible) to answer this question on the basis of PSPC data because of the relatively large errors associated with the hard component temperature; and higher resolution spectroscopy will be needed to resolve this issue. However, we do note that Güdel & Guinan (1995) have suggested that coronal temperatures decrease with increasing age in solar-type (G0–5 V) stars. Their hypothesis is based on an examination of coronal X-ray, EUV, and microwave data for a sample of G stars of significantly different ages.

[7] A small sample of five dMe stars with detected X-ray (*Einstein* IPC) and C IV (*IUE*) fluxes (Linsky et al. 1982) yields a mean value for the ratio of C IV to X-ray emission levels $f_{C\,IV}/f_X \sim 0.02$. Using the same scaling, our measurement of the X-ray flux from GL 411 implies a C IV flux of $\sim 2 \times 10^{-14}$ ergs s^{-1} cm^{-2}, a factor of 2 below the upper limit given by Linsky et al. (1982), thus resolving the apparent contradiction. We further note that the position of GL 411 in the infrared $(J-H)$, $(H-K)$ color-color diagram indicates that it is a metal-poor object (Stauffer & Hartmann 1986). Thus the potential C IV emission in GL 411 would be further diminished by any relative deficiency in its metallicity.

3.2. *Time-resolved Spectroscopy*

All of the dMe stars in our sample exhibit considerable variability in their light curve (see Figs. 2*a* and 2*d*; our X-ray observation of CN Leo is suspected to have been at the beginning of a flare: see Paper I). In order to determine the variation of plasma parameters on these stars we have carried out time-resolved spectroscopy on the two brightest stars in our sample: AD Leo and Wolf 630. We have fitted RS thermal spectra (using XSPEC v.8.5) to counts accumulated in 500 s bins over the duration of the observations; the fitted parameter N_H was constrained to be within the 90% confidence level of the best-fit value obtained from fitting the count spectra obtained from the total duration of the observation, while the parameters T_L and T_H were essentially unconstrained. The resulting best-fit values of the temperature components are however found to remain within $\sim 10\%$ of the high-T and $\sim 50\%$ of the low-T best-fit values obtained from the total data. The best-fit values (and associated 90% confidence intervals) of the low- and high-temperature component emission measures are shown in Figure 2. It appears that the high-T emission components trace the light curves and are the causes of the observed variabilities in count rates, in contrast to the low-T emission components, which are relatively constant and are uncorrelated with the light curves; these impressions are confirmed by fitting[8] straight lines and performing Spearman rank-ordered correlation tests between the emission measures and the count rates (see Table 4).

More rigorous Bayesian techniques confirm the above results: For AD Leo and Wolf 630 respectively, the low-T components are ~ 8000 and ~ 40 times more probable to be steady than correlated with the light curves, while the high-T components are, respectively, $\sim 10^{21}$ and $\sim 10^{19}$ time more probable to be correlated with the light curves (Kashyap 1995).

4. MODELING

The well-established occurrence of thermal inhomogeneities, analogous to solar features such as spots and plages, on late-type stars provides the underlying rationale for the assumption that magnetic field structures similar to solar coronal loops are also fundamental features of stellar coronae. Previous investigations of the applicability of loop models to the interpretation of the observation of emission from hot plasma in the atmospheres of late-type stars include Schmitt et al. (1985), Giampapa et al. (1985), Stern, Antiochus, & Harnden (1986), Schrijver, Lemen, & Mewe (1989), and Schmitt (1990) among others.

The direct detection of strong (~ 3–4 KG) magnetic fields on the surfaces of dMe stars (Saar & Linsky 1985) adds to the plausibility of the hypothesis that X-ray emission in late-type dwarfs arises, at least in part, from structured loop atmospheres. In the following, we will construct coronal loop models for the observed X-ray coronae.

[8] The probability distributions describing the fit parameters are asymmetric. We estimate an effective standard deviation in interpolating between the 90% confidence intervals.

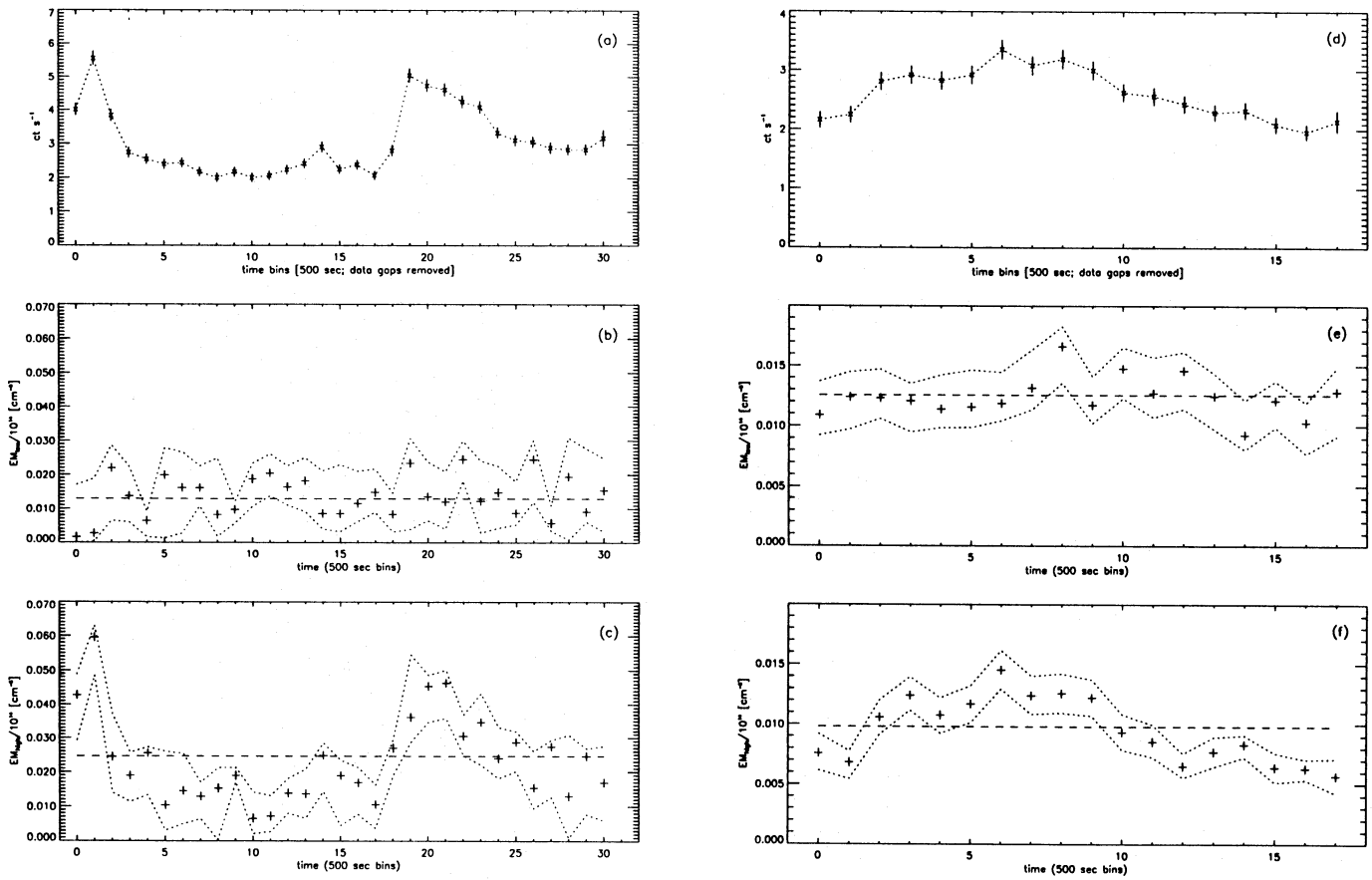

FIG. 2.—Time-resolved spectroscopy of AD Leo and Wolf 630. The data have been binned into equal time intervals of 500 s (except the last bin). Gaps in the data stream have been ignored for purposes of clarity, i.e., the abscissa is not linear in time. Note that only the high-T emission measure component shows significant temporal cross-correlation with the X-ray light curve, strongly suggesting that it is the high-T component that is principally responsible for the observed X-ray variability. (*a*) The X-ray count rate light curve for AD Leo in the 0.2 keV passband. (*b*) The emission measures of the low-temperature component (+signs) along with the 90% confidence intervals (*dotted line*) for the same binning as (*a*). (*c*) As (*b*), but for the high-temperature emission measure component. (*d*) The X-ray count rate light curve for Wolf 630 in the 0.2–2 keV passband. (*e*) As (*b*), but for Wolf 630. (*f*) As (*c*), but for Wolf 630.

TABLE 4

STATISTICAL TESTS ON TIME-RESOLVED EMISSION MEASURES

A. Correlation with Light Curve

Star	Component	Correlation[a]	Significance[b]
AD Leo.....	High-T	0.83	$\ll 0.001$
	Low-T	−0.04	0.83
Wolf 630.....	High-T	0.96	$\ll 0.001$
	Low-T	0.19	0.48

B. Constancy of Emission Measures

Star	Component	Slope[c]	Reduced χ^2	Goodness-of-fit[d]
AD Leo.....	High-T	0.0002 ± 0.0001	5.5	$\ll 0.001$
	Low-T	0.00007 ± 0.0001	1.38	0.08
Wolf 630.....	High-T	-0.0002 ± 0.00004	5.4	$\ll 0.001$
	Low-T	-0.00001 ± 0.00007	1.07	0.38

[a] Spearman rank-ordered correlation coefficients.

[b] The significance of the correlation measures the probability that uncorrelated quantities would show the observed correlation by chance.

[c] The slope of the straight line obtained by a least-squares fit.

[d] The goodness-of-fit measures the probability that a value of χ^2 as poor as observed would occur by chance.

4.1. *Analytical Loop Models*

As a prelude to the construction of semiempirical loop model atmospheres based on the data and the application of a fully general numerical code, we recall the basis for the simplest models of stellar X-ray coronae, namely the analytical scaling laws derived by RTV, and extended by Serio et al. (1981). In this picture, the stellar corona consists of a complex of loops of magnetically confined plasma; the energetics of individual loops then imposes a constraint on the relation connecting the loop's geometry and its thermal plasma characteristics, encapsulated by the RTV scaling law

$$T_M = 1.4 \times 10^3 (pl)^{1/3} \text{ K} , \quad (1)$$

where T_M, p, and l are the loop apex temperature, base pressure, and loop semilength, respectively. Equation (1) is applicable to loops in quasi-hydrostatic equilibrium; this scaling also presumes that the gas pressure is spatially uniform, e.g., that the loop length is less than the local pressure scale height s_p,

$$s_p = 6 \times 10^3 T_M (R_*/R_\odot)^2 (M_*/M_\odot)^{-1} , \quad (2)$$

where we assume a fully ionized plasma; the emission scale height, s_{em}, is half the pressure scale height, $s_{em} = s_p/2$.

Because of the nearly isothermal temperature distribution in the coronal portion of such loops (a result of the highly efficient nature of thermal conduction at temperatures above 10^6 K), the apex temperature is close in value to the spatially averaged coronal loop temperature; hence, we shall consider T_M as a reasonable proxy for the mean coronal temperature within the loop structure. We further note that the analytical model can be readily extended to loops longer than the pressure scale height; in that case, equation (1) is simply modified by a multiplicative term, determined by Serio et al. (1981),

$$T \approx 1.4 \times 10^3 (p_0 l)^{0.33} \exp [-0.04 l (2/s_H + 1/s_p)] \text{ K} , \quad (3)$$

where p_0 is the base pressure of the loop and s_H is the energy deposition scale height. (We note as an aside that the RTV scaling is insensitive to the geometric properties of the loop heating; that is, the scaling is virtually unchanged in cases of highly nonuniform heat deposition, mainly due to the effects of rapid [efficient] heat redistribution by thermal conduction; Withbroe 1978.)

As an aside, we note that an additional freedom provided by models such as those of Serio et al. is the possibility of "broadening" loops as they lift above the solar surface; in this way, the areal filling factor would be a function of height above the solar surface. In the present context, this additional degree of freedom for loop models has the primary effect of changing the hot-to-cool emission measure ratio. Based on the data used here, we are not in the position to constrain this degree of freedom, and hence we do not use it in our further modeling. Moreover, the RTV scaling law is only weakly dependent on changes in the loop cross section with height (Vesecky, Antiochus, & Underwood 1979). In any event, Klimchuck et al. (1992) find on the basis of a quantitative analysis of *Yohkoh* SXT (Soft X-ray Telescope) images that solar coronal X-ray loops do not expand with height.

Finally, the loop lengths follow from the RTV scaling law (eq. [1]) and the constraint that the integrated emission from loops correspond to the observed X-ray luminosity, i.e.,

$$l = 2.16 \times 10^{16} (R_*/R_\odot)^2 T^{7/2} L_X^{-1} f \text{ cm} , \quad (4)$$

where f is a geometrical parameter representing the filling factor of loops.

The simplest question one can now ask is whether these scaling laws have any relevance to our observations. One elementary consistency check is to see whether the loop lengths implied by inserting the derived values of L_X and T for the two-temperature components into equation (4) give loop dimensions that are indeed smaller than the pressure scale height. Using the results provided in Tables 1–3, one can readily show the following:

1. The low-T emission component is characterizied by loop scale lengths substantially smaller than the corresponding pressure scale height; thus, these loops are consistently described by the RTV scaling laws.
2. The high-T emission component is characterized by loop scale lengths of order of, or larger than, the corresponding pressure scale height, *unless* the corresponding filling factor is much smaller than unity. Thus, if $f \sim 1$ for this component, then these loops are *not* consistently described by the simple RTV scaling laws.

It would be interesting to compare these results for M dwarfs with the results from earlier work for F and G dwarfs by various authors. We note that previous modeling efforts have been characterized by diverse approaches and data sets. The general consensus, however, is that coronal temperatures extending in range from a few times 10^6 to $\sim 10^7$ K along with loop lengths that are quite small compared to the stellar radius are present, at least in the coronae of active G dwarfs. However, significantly more extended loop configurations have also been found to be consistent descriptions of some stellar coronae. For example, Stern et al. (1986) find that the coronae of active dwarf F and G stars are best represented by a single component with $T \sim 10^7$ K. The best-fit loop models have loop lengths comparable to the stellar radius. By contrast, Giampapa et al. (1985) utilize single-component loop models but with a surface filling factor included to fit the observed X-ray emission for an assortment of active and relatively quiescent G–K dwarfs; the estimated loop lengths were generally less than a few percent of the stellar radius for loops with maximum temperatures of a few times 10^6 and filling factors less than unity. Schrijver et al. (1989) did adopt a two-component model approach but also included a geometrical expansion factor describing the expansion of loops with height in the atmosphere. These investigators find for the active G dwarf σ^2 CrB that a hot ($T \sim 3 \times 10^7$ K) and a cool ($T \sim 5 \times 10^6$ K) component are required to describe the observed X-ray emission with upper limits to the loop lengths of $L/R_* < 3$ and $L/R_* < 0.06$, respectively.

We performed an analysis of the PSPC pulse-height spectrum of the active solar-type star π^1 UMa (G0 V) following the methods discussed below. We found that the best-fit loop model consists of two thermal components with temperatures of 1.5×10^6 K and 6.1×10^6 K, respectively. Convergent solutions for the "hot" component in our model for π^1 UMa exhibit loop lengths that are an appreciable fraction of the stellar radius ($\sim 40\%$) while the lower temperature component appears to be compact ($\sim 5\%$ of the stellar radius). Neither component is variable at a level of about 20%.

Our results for the M dwarfs require a more detailed examination of the models; this is done in the following subsection.

4.2. *Semiempirical Loop Models: Methods*

To go beyond the previous analyses based on simple scaling requires a detailed comparison of the X-ray data with predictions derived from numerical models of loop atmospheres. We have carried out such an analysis, based on the solution of the one-dimensional single-fluid momentum and energy equations for a quasi-static "loop atmosphere," based on numerical methods described some time ago by Rosner & Vaiana (1977). These solutions are obtained by means of straightforward integration of the corresponding ordinary differential equations, using a fourth-order adaptive Runge-Kutta scheme; and have been used here, in conjunction with spectral analysis results, to estimate loop parameters for our program stars. Our analysis was carried out by constructing loop models for a grid of values of the loop semilength l, and base pressure p_0, using an appropriate metallicity Z (see Appendix A). For each pair of values (l, p_0), we determine the maximum temperature of the loop T_{max}, and the surface flux from the semiloop,

$$f_X = \int n_e(s)^2 P[T(s), Z]\, ds \equiv < n_e^2 P(T, Z) > l\,, \qquad (5)$$

where $\langle n_e^2 P(T, Z)\rangle$ is an average emission from the loop, and in turn allows us to estimate the observable X-ray luminosity of these stars, or

$$L_X = f_X 4\pi R_*^2 f q(l/R_*)\,, \qquad (6)$$

where the geometry factor q is given by the expression (see Schmitt 1990; Kashyap et al. 1992)

$$q(x) = \frac{1}{2x}\left[x + x^2 + \frac{1}{3}(2x + x^2)^{3/2}\right]. \qquad (7)$$

This factor takes into account effects such as the shadowing of coronal emission by the star. The (surface) filling factor f measures the area of the sellar surface covered by the basal area of the loops. We adopt $f = 1$ unless noted otherwise. The resulting values of T_{max} and L_X may be compared to the spectral fit parameters[9] (see Fig. 3); the intersection of the regions of the (l, p_0) grid where the computed and observed values of L_X and T_{max} "match" denote the possible loop solutions. Since L_X and T_{max} are not perfectly well known, but instead have associated uncertainties, we actually obtain for each stellar X-ray observation a strip in the (l, p_0)-plane within which lie all solutions that satisfy the observations at the specified confidence level.

4.3. *Semiempirical Loop Models: Comparisons with Data*

Using the method outlined above, we have constructed the loci of possible solutions in the (l, p_0)-plane for every one of our program stars which had sufficient counts to enable a spectral fit; the results are shown in Figure 3. The main conclusions are as follows.

(i) We find that the low-temperature components can be systematically modeled with loops of small length (e.g., $l \ll R_*$) and high base pressure (e.g., $p_0 > p_{0\odot}$). This result is consistent with our previous finding from scaling analysis that the low-temperature component can be well-modeled using the simple RTV loop scaling laws.

(ii) The high-temperature components can be modeled by loops which are very large ($l \sim R_*$) and have moderately high base pressure ($p_0 \sim 20$ dnes cm$^{-2} \gg p_{0\odot}$), under the assumption of filling factors $\sim O(0.1)$. This behavior is very unlike what is found for the Sun: comparable solar coronal structures are typically associated with "compact loop flares" (see Pallavicini, Serio, & Vaiana 1977), whose size is similar to that of typical active region loops. The substantially larger scale "long-enduring events" associated with filament disruptions instead tend to have systematically lower temperatures and pressures, and are therefore not natural counterparts to the stellar high-T component we are now discussing. We also not that there is a further consistency requirement involving the low-T component: Since the low-temperature component is always present, and clearly takes up a significant fraction of the coronal volume, it cannot be that the high-temperature component filling factor is close to unity.

(iii) The aforementioned high-T solutions are not consistent with the RTV scaling laws because their dimensions violate the constraint that the loop length be smaller than the pressure scale height; this result again corresponds to what we found in the previous subsection.

(iv) It *is* possible to construct a model for the stellar high-temperature component which makes contact with the solar case *if* one assumes very small filling factors for the emitting volume; this model consists of loops which have very high base pressures $p_0 > 100$ dynes cm^{-2}. Since the emission measure is not affected by changing the filling factor, the immediate implication is that the emitting volume must consist of a superposition of well-dispersed small emitting structures (perhaps analogous to loop flares and the flaring bright points seen at X-ray wavelengths; see Golub et al. 1974; Golub 1992).

We can make sense of these results if we consider again our time-resolved spectroscopy analyses for AD Leo and Wolf 630 discussed above. Recall that for these stars, the low-T emission components are relatively steady; this, together with our above results, argues strongly that this component may be fruitfully modeled as comprised of a large number of static coronal loops covering the entire stellar surface. In contrast, our temporal analyses show that the high-T components are variable; such an atmosphere cannot be consistently modeled by quasi-static structures (RTV) and is more sensibly associated with a superposition of emission from flaring coronal structures.

To summarize the above: our modeling indicates that a consistent picture of coronal emission from low-mass stars can be constructed which retains close contact with ideas developed in the solar context. In brief, we find that these coronae are well-represented by two distinct thermal structural components: a low-temperature component, whose emission is consistent with a constant source; and a high-temperature component whose emission is inconsistent with source constancy. From previous work, it is well-known that PSPC spectra can also be fitted with a single component which allows for a range of plasma temperatures within that single component (e.g., a model based on a power-law differential emission measure; see Schmitt et al. 1990); in the present context, our observation of emis-

[9] As pointed out by Maggio & Peres (1995), the estimated plasma temperature is not T_{max}, but an average over the loop. However, the error bars we quote on the best-fit temperatures encompass the loop T_{max} even if their suggested corrections apply. Hence, we take the temperatures derived from spectral fits to be measures of the loop maximum temperatures. This assignment has no effect on the discussion below.

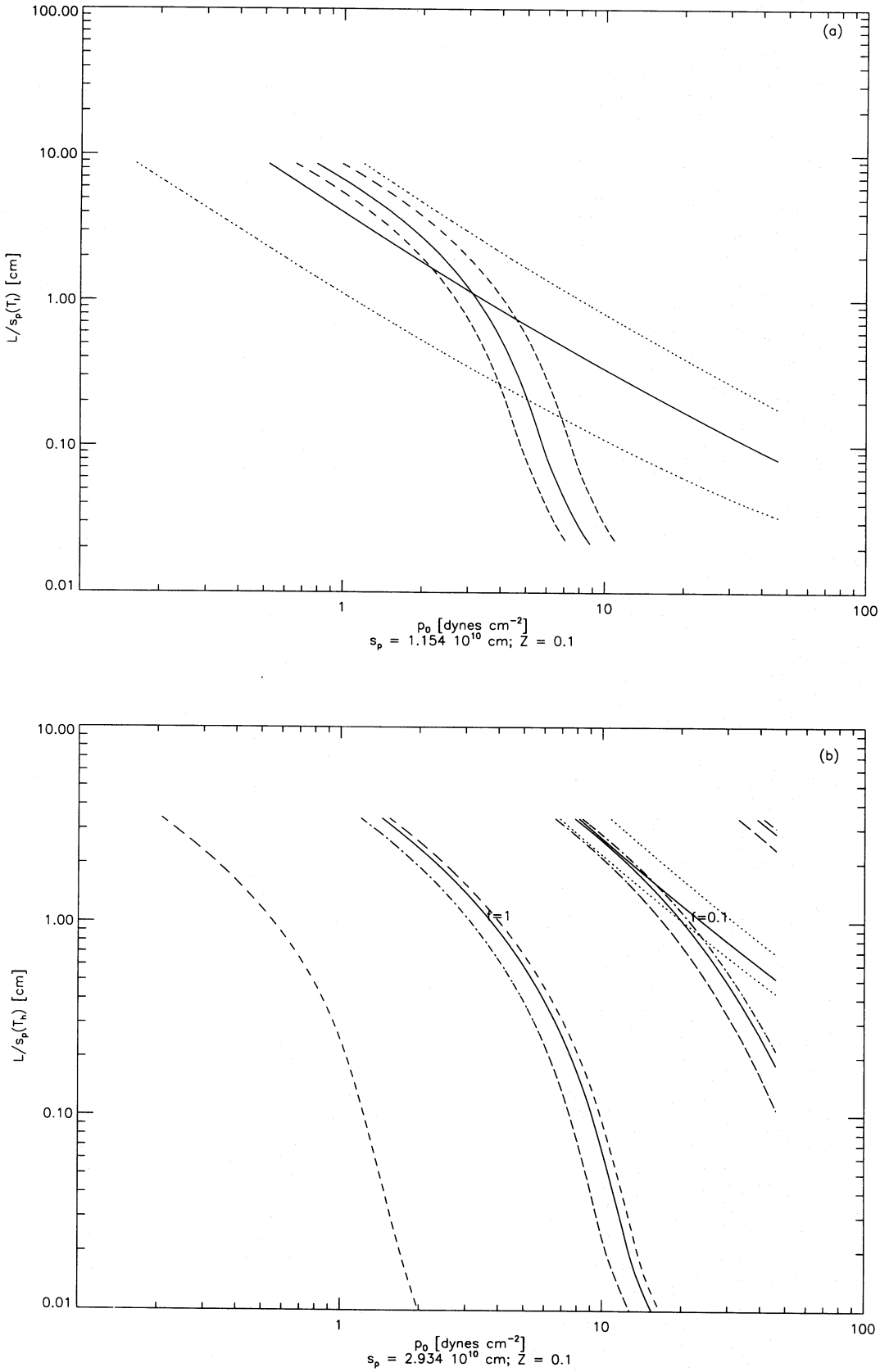

FIG. 3.—Results of loop modeling. We plot the locus of loop atmosphere solutions which satisfy the observational constraints of luminosity and temperature in the $l - p$ plane. The dotted lines enclose the region in the $l - p$ plane which give rise to the observed temperature range, while the dashed lines enclose the region which give rise to the corresponding observed luminosity; the solid lines within represent the loci of the best-fit T and $EM(T)[P(T, Z)]$, respectively. The filling factor is taken to be 1 unless explicitly stated otherwise. (*a*) The low-T ($=3.5 \times 10^6$ K) component of AD Leo. (*b*) The high-T ($=8.9 \times 10^6$ K) component of AD Leo; ranges of $L_{X,h}$ obtained for $f = 1$, 0.1, 0.01 are plotted. (*c*) As (*a*), for Wolf 630 ($T_{low} = 1.97 \times 10^6$ K); (*d*) As (*b*), for Wolf 630 ($T_{low} = 9.12 \times 10^6$ K); (*e*) As (*a*), for GL 406 ($T_{low} = 1.71 \times 10^6$ K); (*f*) As (*b*), for GL 406 ($T_{high} = 8.23 \times 10^6$ K); (*g*) As (*a*), for VB 8 ($T_{low} = 1.5 \times 10^6$ K); (*h*) As (*b*), for VB 8 ($T_{high} = 8.71 \times 10^6$ K); (*i*) As (*a*), for GL 411 ($T_{low} = 1.3 \times 10^6$ K); (*j*) As (*b*), for GL 411 ($T_{high} = 6.68 \times 10^6$ K); (*k*) As (*b*), for GL 699 ($T_{high} = 2.3 \times 10^6$ K).

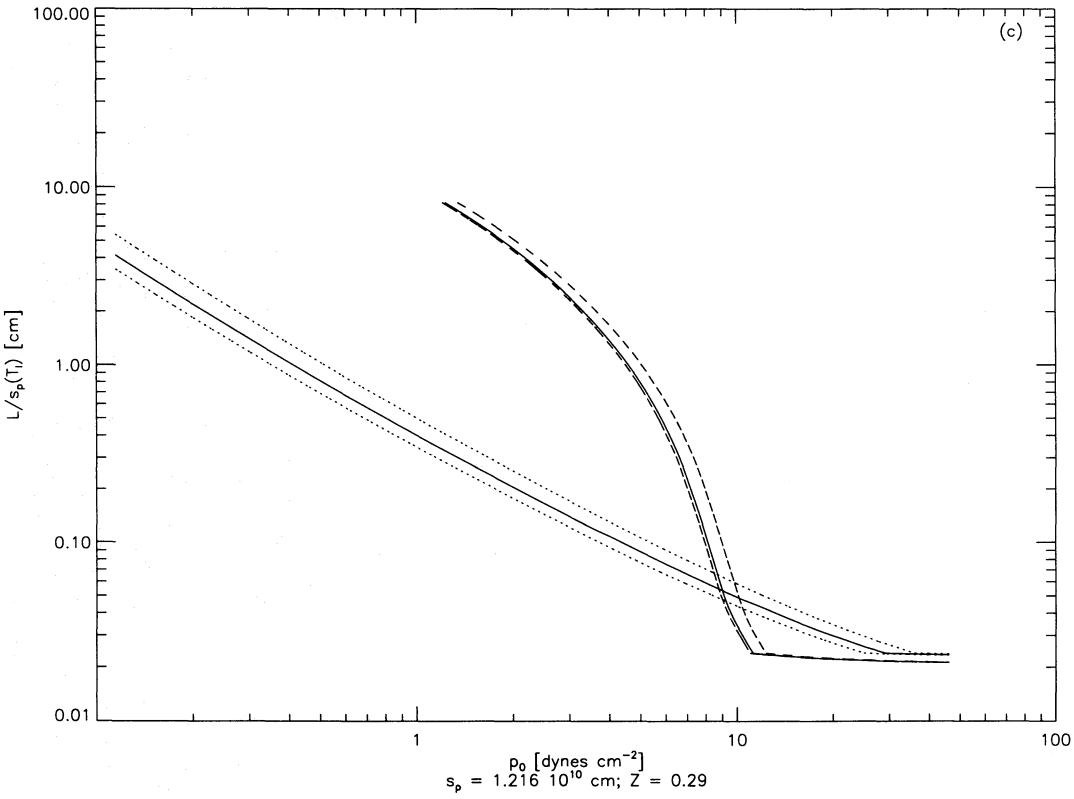

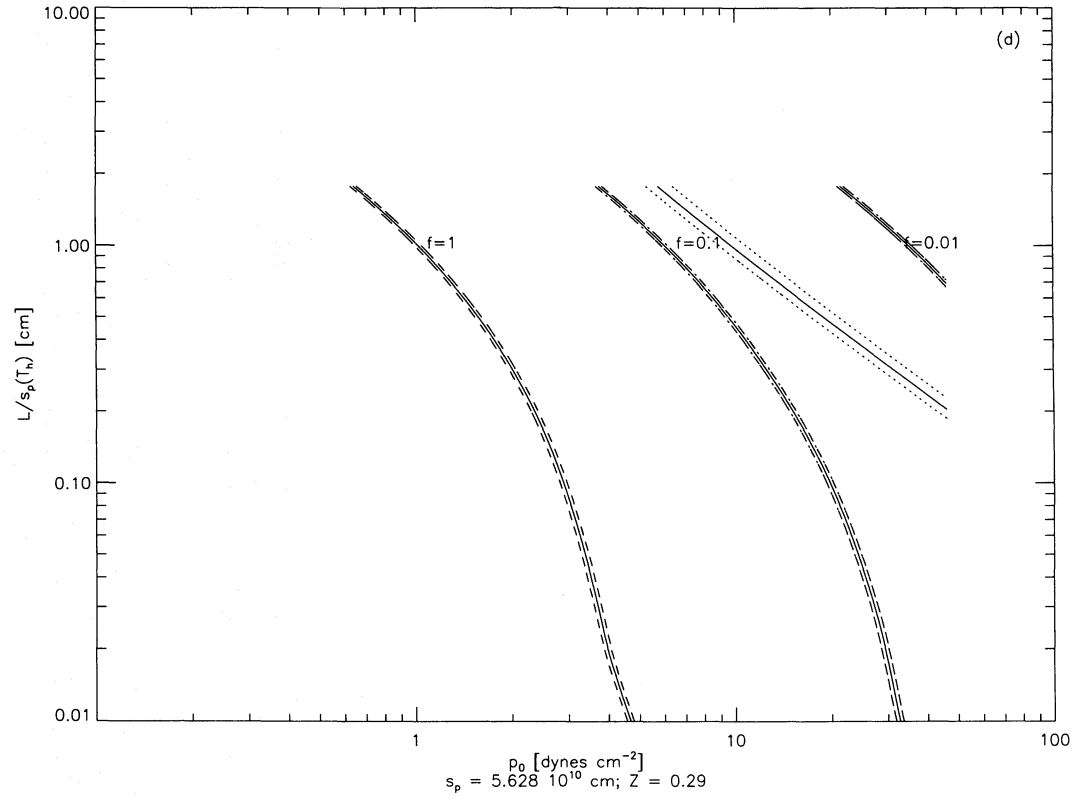

FIG. 3—*Continued*

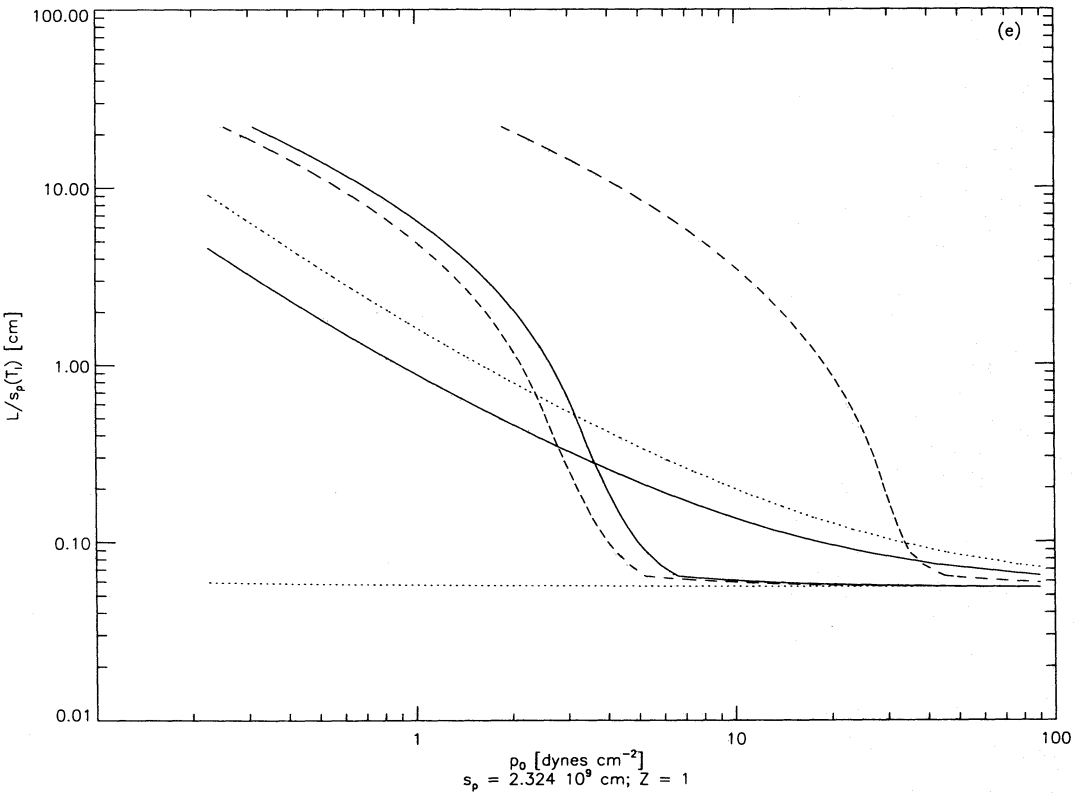

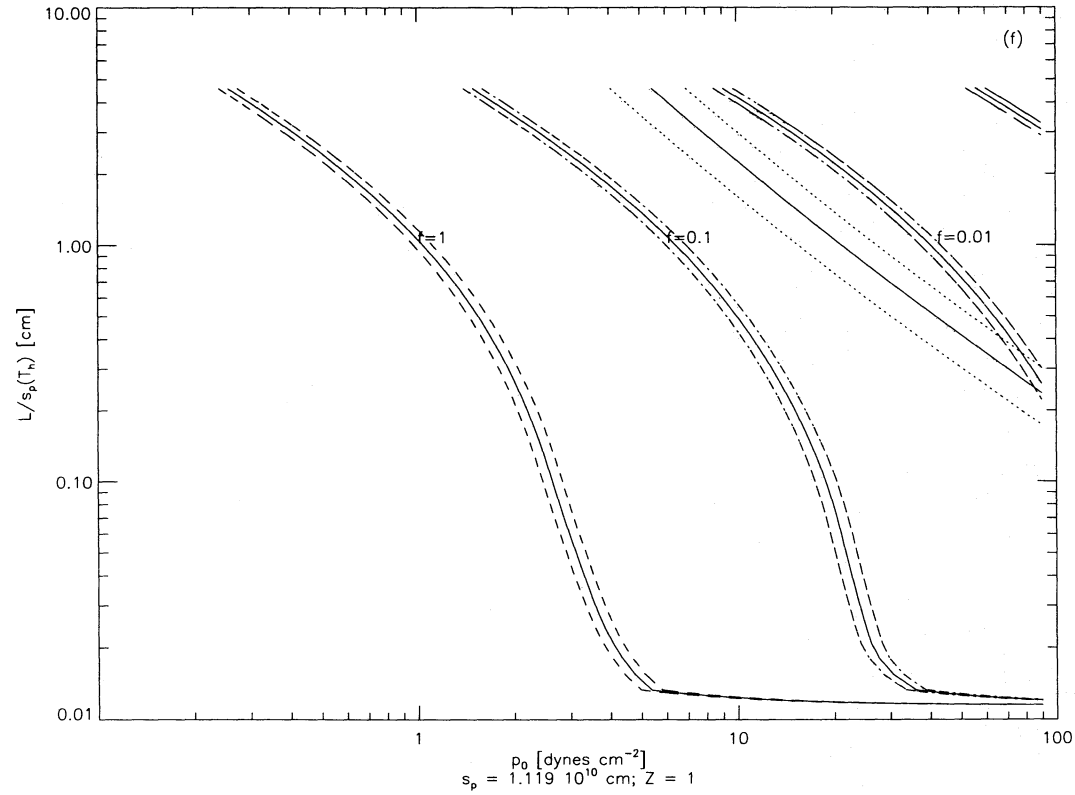

FIG. 3—*Continued*

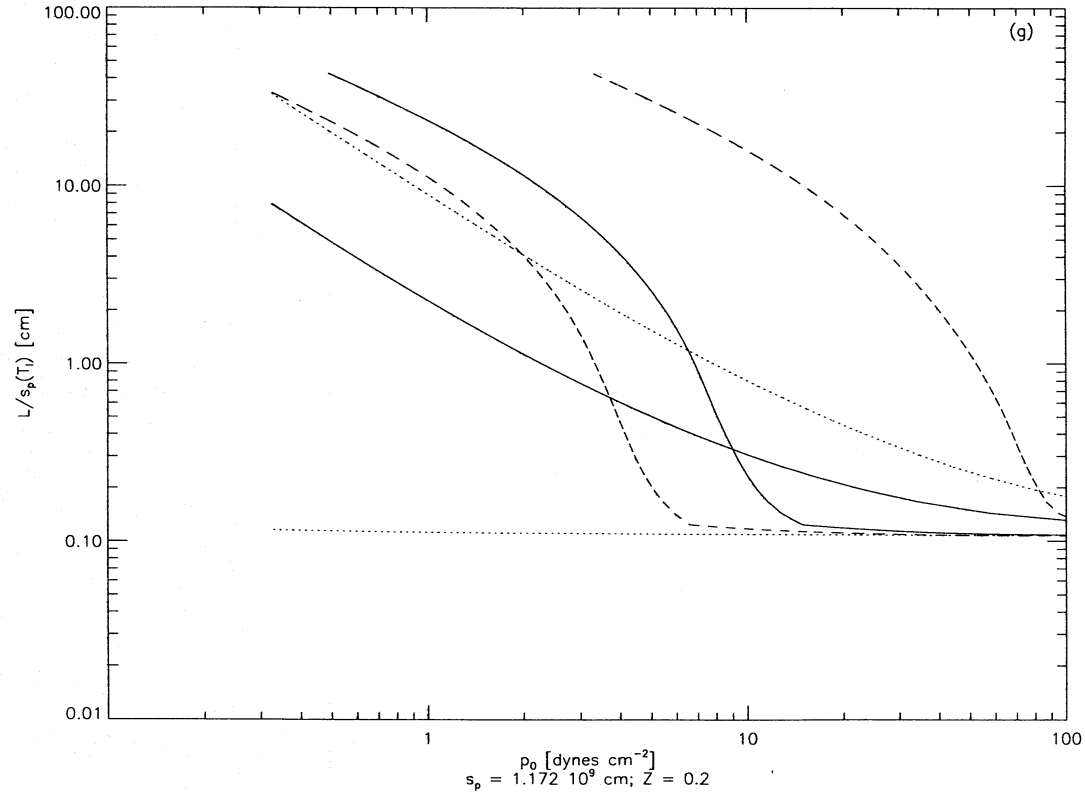

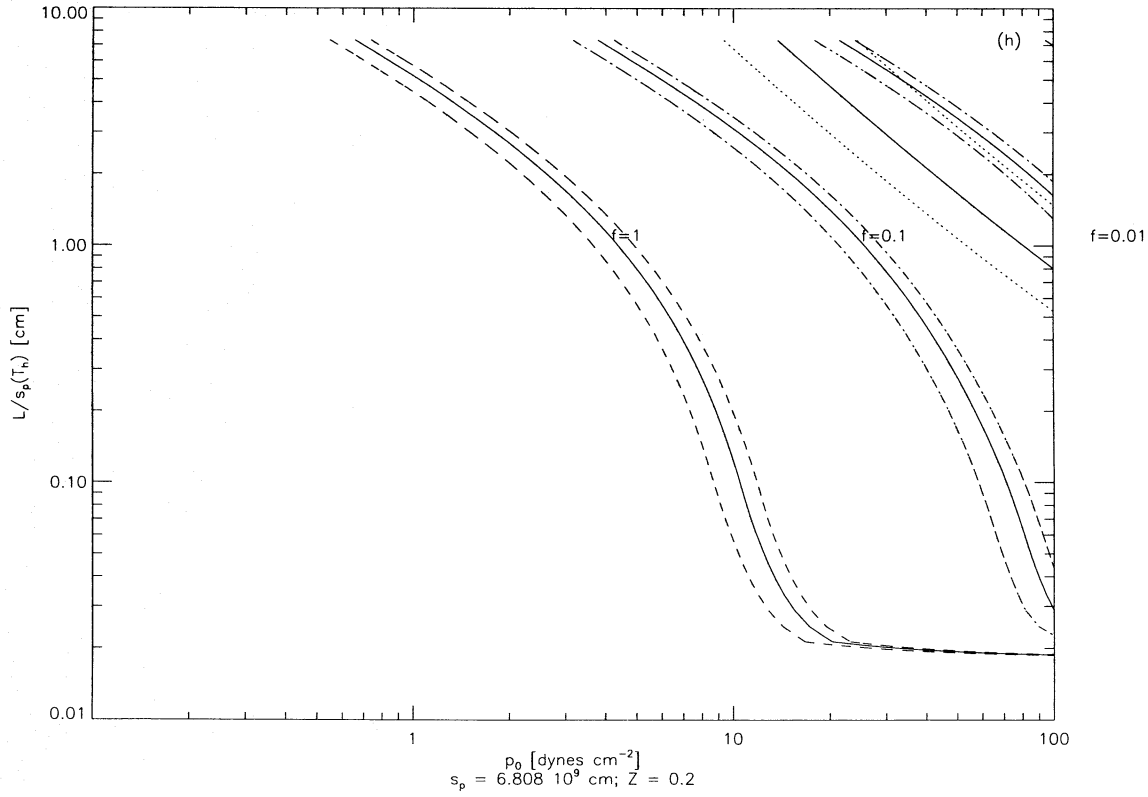

FIG. 3—*Continued*

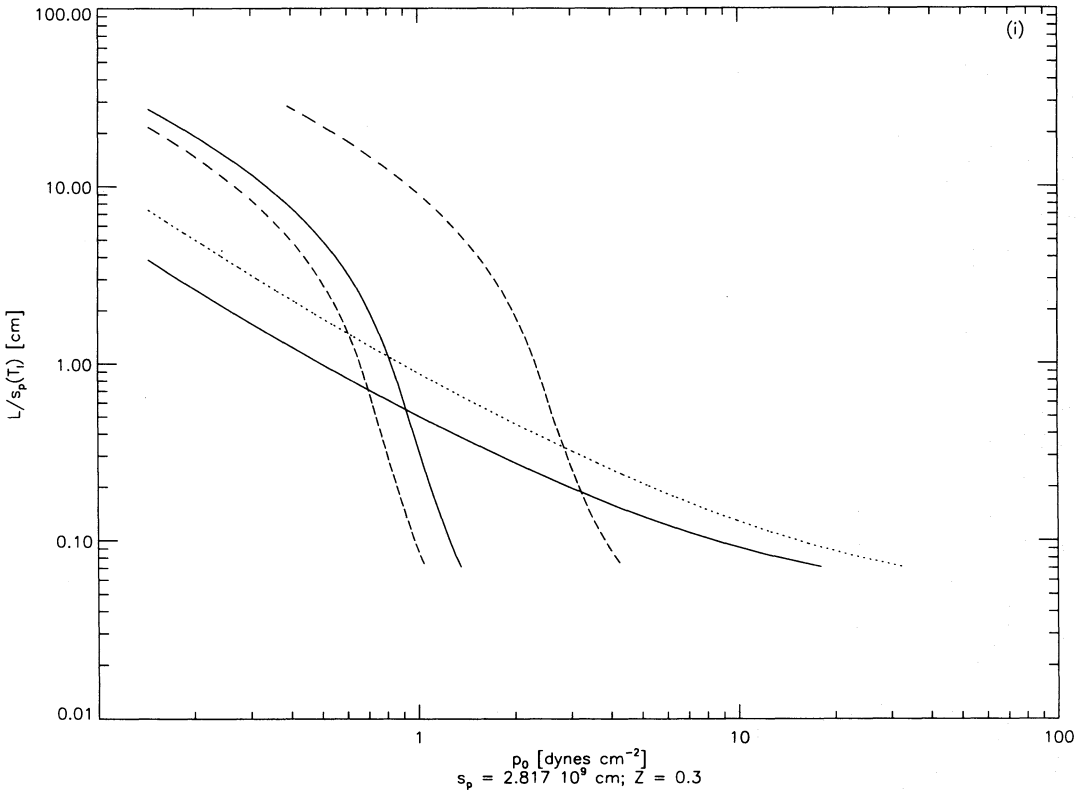

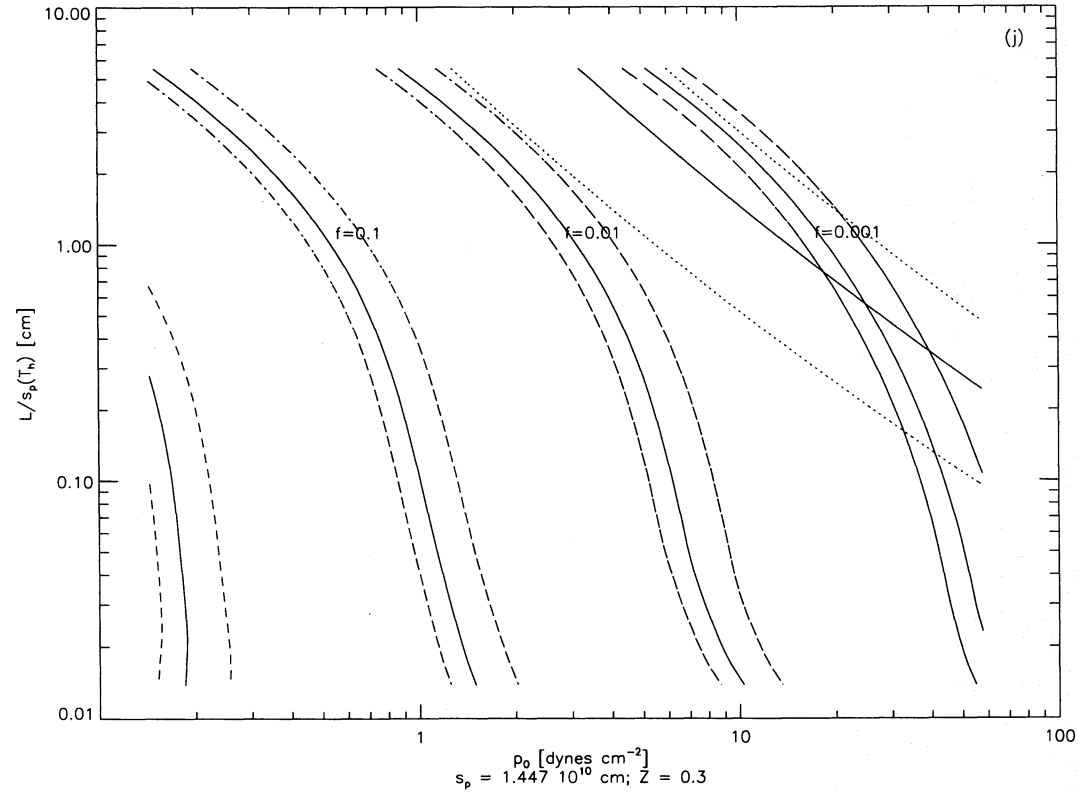

FIG. 3—*Continued*

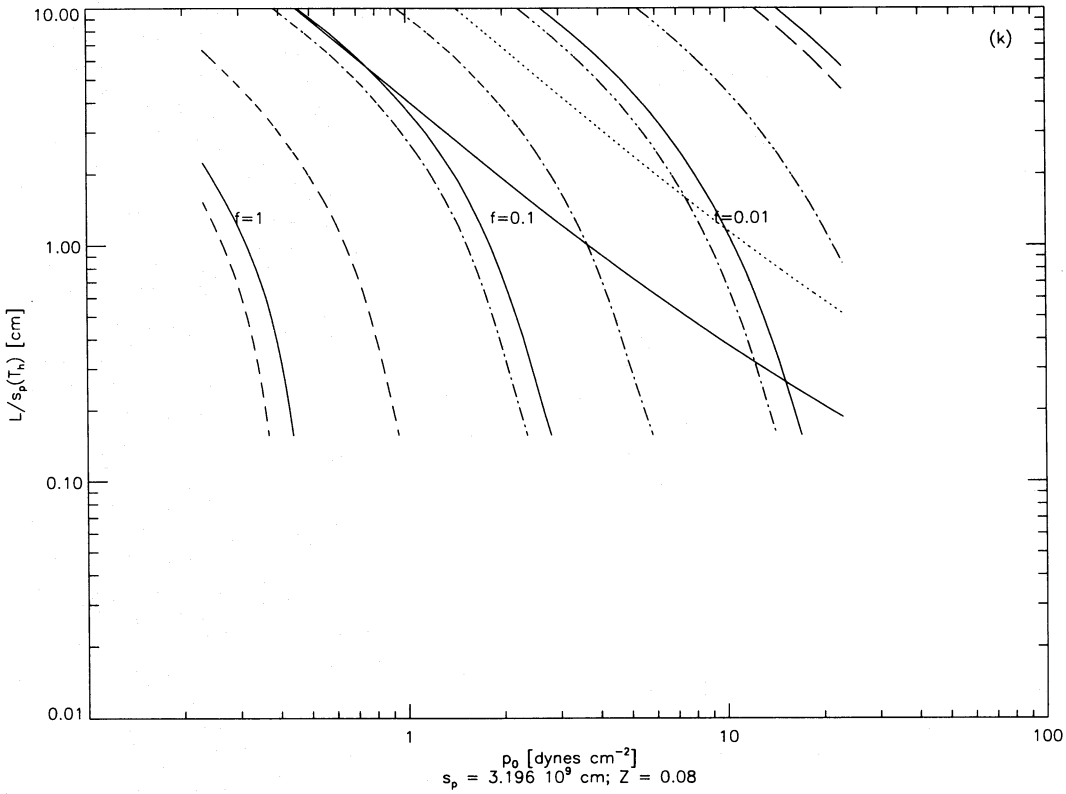

FIG. 3—*Continued*

sion variability implies that this component would have to be itself variable in intensity and in its emission measure distribution. While we cannot exclude this type of model, we prefer the two-component model because it is simpler, and because it offers a more elegant explanation of the observations in terms of the solar analogy. In particular, we suggest that the low-temperature component may be interpreted as a superposition of emission from quasi-static loop structures, analogous to a combination of quiet Sun and quiescent active region loops; and that the high-temperature component may be ascribed to emission from rapidly emerging, highly active, magnetic flux structures, whose activity is possibly related to magnetic field reconnection and annihilation during the emerging process, leading to a superposition of transient or flare events which is variable in time. These associations are consistent with the derived temperatures for the stellar emission components in the sense that the low-temperature component does correspond to observed temperatures in solar quiet Sun and quiescent active region loops; and the high-temperature component does correspond to observed temperatures in flaring solar loops. Finally, we reemphasize that it is also possible to construct more complicated models. These are not preferred by us because they do not satisfy Occam's razor of simplicity.

5. SUMMARY AND DISCUSSION

5.1. *Coronal Characteristics of Low-Mass Stars*

One of our principal conclusions is that if the observed X-ray emission of low-mass stars is represented by two distinct temperature components, then the low-temperature component can be consistently described by a model in which the emitting loops are quiescent, and are relatively small ($l < s_p$); this result is consistent with the application of the RTV scaling laws to this component. These conclusions are also consistent with, for example, the earlier results of Haisch et al. (1990), who utilized *EXOSAT* LE observations of the low-energy X-ray emission from the M dwarf eclipsing binary YY Gem to conclude that the bulk of the low-energy X-ray emission arises in relatively low lying loops close to the stellar surface. This interpretation is supported by *ROSAT* observations of YY Gem, which exhibits deep minima coinciding with primary and secondary optical minimum (see Schmitt 1994).

One obvious question is whether the basic scheme of attributing the observed emission to two distinct emission components characterized by different mean temperature distributions is valid. In the solar case, this type of separation is usually identified physically with three X-ray components: The quiet Sun [$T \sim 2 \times 10^6$ K, filling factor $\sim O(1)$], active regions ($T \sim 3 \times 10^6$ K, filling factor < 1), and a highly variable component identified with flares ($T \gtrsim 10^7$ K, filling factor $\ll 1$); in the solar case, the emission measures of the quiet Sun and of active regions are often fairly comparable in magnitude despite the significant difference in filling factors (e.g., Vaiana & Rosner 1978). Now, the key points are, first, that photon energy-sensitive detectors such as the *ROSAT* PSPC are not capable of cleanly separating the quiet Sun and active region components because their temperatures are too similar, given the limited energy resolution of this type of detector. Hence, the minimal conclusion we can draw is that the stellar low-temperature component we see is a superposition of emission from quiet Sun and quiescent active region-like structures. However, our analysis of the implied loop dimensions suggests that most of the low-T emission we see comes from active region-like structures; the reason for this

conclusion is that in the solar case, quiet Sun structures not only have large filling factors, but are also geometrically large (i.e., quiet Sun loop structures are typically of the order of, or larger than, their pressure scale height; RTV). Furthermore, there is evidence from an analysis of *EUVE* observations of Procyon (Schmitt, Haisch, & Drake 1994) and ϵ Eri (Schmitt et al. 1996) that the low-T component in this object is associated with active region emission (Schmitt, Haisch, & Drake 1994).

Further independent support comes from observations of stars in the UV, such as reported in a study of transition region lines in the spectrum of the dM0e flare star AU Mic, carried out with the Goddard High Resolution Spectrograph on board the *Hubble Space Telescope* (Linsky & Wood 1994); these authors find that two components are necessary to account for the observed C IV and Si IV line profiles: These profiles can be fitted by two gaussians, one a narrow component whose line width is similar to those seen in solar active regions and quiet Sun, and a broad component reminiscent of the broad C IV profiles observed in solar transition region "explosive" events; the latter are believed to be associated with emerging magnetic flux regions, where magnetic field reconnection (and flaring) occurs. Thus, the data from both the Sun and other stars support our contention that the relatively quiescent, low-temperature emission measure component we see in our low-mass star data is best interpreted as combined quiet Sun/quiescent active region emission, with a dominant contribution from quiescent active regions; and that the variable, high-temperature, component is associated with compact flaring structures.

5.2. *Implications for Stellar Dynamo Theory*

Our conclusions in the preceding section that the coronal geometry for low-mass dwarf stars is dominated by relatively compact loop configurations, and that the emission contribution of structures with a large-scale dipolar or quadrupolar geometry is negligible, has significant implications for dynamo theory.

The key question is, why is all of the emission, from both the low and the high-temperature components, coming from relatively compact coronal loops? In the solar case, it is the large-scale surface magnetic structure that is the principal tracer of solar magnetic dynamo activity, and which carries both the spatial and temporal signatures of the 11 yr solar activity cycle. Compact loops are typically associated with emerging flux regions, i.e., active regions and compact flare loops are usually thought to reflect magnetic reconnection processes triggered as part of this flux emergence process; in contrast, the larger scale structures associated with quiet regions, coronal holes, and the like are associated with the (turbulent) diffusion process linked to the large-scale solar magnetic dynamo. Our observations suggest that X-ray emission from the stellar equivalent of solar large-scale structures is absent on these stars. This could be because either such structures, although present, simply do not emit X-rays, or because they are not present at all. If we adhere to the solar analogy, we are led to adopt the second possibility: on the Sun, all structures that are present—independent of characteristic site—are "energized" and either emit radiation (i.e., "closed" structures) or wind outflows ("open" structures/coronal holes). In other words, we take the absence of emission from large-scale structures as evidence that such structures do not exist. However, these large-scale structures are—in the solar case—tracers of its large-scale (i.e, solar radius scale) magnetic field structure (see Sheeley 1981). Their absence for the M dwarfs considered in this study suggests that these stars do not possess a large-scale magnetic field structure. It is this large-scale field structure for which "classical" (α-ω) dynamo theory seeks to explain. We therefore suggest that "classical" dynamo action does not take place in these stars.

Rosner et al. (1995) have discussed some of the reasons why large-scale ("classical") dynamo activity might be suppressed, and replaced by small-scale dynamo activity, in the context of X-ray emission from hybrid stars; in that case, the classical dynamo process can be shut off if the magnetic dynamo number falls below its critical value for linear instability as a star evolves. In the present case, the switch-off of classical dynamo action may instead occur because, as a star becomes fully convective, the shear zone now believed to lie at the base of the convection zone disappears. As a result, the "shell dynamo" commonly thought to operate in solar-like stars can no longer function (see Rosner & Vaiana 1980). One is then faced with the conundrum that fully convective stars are nevertheless observed to be magnetically active. Rosner et al. (1995) point out that even in the absence of "classical" dynamo action, it has been long known that small-scale dynamo action is nevertheless possible in highly turbulent fluids (Meneguzzi, Frisch, & Pouquet 1981; Vainshtein & Kichatinov 1986). This type of dynamo action does not depend on the nonvanishing of the mean fluid (kinetic) helicity $\langle \boldsymbol{u} \cdot \nabla \times \boldsymbol{u} \rangle$; and leads to the generation of magnetic fields on the spatial scales of the turbulent flow field, i.e., small spatial scales (as opposed to fields on the scale of the star itself). Durney, De Young, & Roxburgh (1993) have discussed a similar scenario; we note, however, that it is not obvious that it is the absence of a region of weak buoyancy that suppresses classical dynamo action (as Durney et al. argue)—after all, the interior of a fully convective star near its center is very weakly convectively unstable. Instead, it seems more plausible that it is the absence of a large-scale shear zone, where significant large-scale flux amplication can take place, that is the decisive difficulty. In any case, this issue is not likely to be resolved until numerical experiments can be carried out to test these ideas.

Finally, one might ask why these active stars seem to have a larger fraction of their equivalents of active region loops in a flaring state than is the case for the Sun. On the Sun, such compact flare loops are especially prominent during the early life of active regions, i.e, when active region evolution is dominated by flux emergence, and by a predominance of smaller, more compact, loop configurations. On the basis of other considerations, we argue that surface flux evolution for these stars is most likely dominated by flux emergence and submersion (as opposed to flux emergence and turbulent diffusion); this suggests in the present context that the surface of these late-type stars is covered by regions similar to solar active regions during the early stages of rapid flux emergence, e.g., a period of vigorous surface activity and substantial loop flaring, a picture which comports with our naive notions of what it would mean for a star to be magnetically more active.

5.3. *Spin-Down of Low-Mass Main-Sequence Stars*

Our result that the emission from both the high- and low-temperature components in the dMe stars comes from

relatively compact coronal structures also suggests a natural explanation for the observed mass dependence of angular momentum evolution in late-type, main-sequence stars: That is, we know from observations that the lowest mass stars spin down more slowly than the more nearly solar-type stars (Stauffer & Hartmann 1987). Moreover, there is little difference between the levels of chromospheric emission from the lowest mass stars thus far observed in the Pleiades and Hyades (Stauffer, Liebert, & Giampapa 1995) even though these two clusters differ in age by roughly an order of magnitude. The same phenomenon is also observed in the X-ray regime, where there is little change in the X-ray properties of the M dwarfs from the young α Per cluster (see Randich et al. 1995), to the Pleiades (see Stauffer et al. 1994) and the Hyades (see Stern, Schmitt, & Kahabka 1995a) while, by contrast, the X-ray output of the more massive G and K dwarfs decreases by more than an order of magnitude. This suggests—given the well-established relation between stellar rotation and stellar activity level (e.g., Pallavicini et al. 1981)—that there has been relatively little rotational evolution (i.e., spindown) between the age of the Pleiades ($\sim$79 Myr) and the age of the Hyades ($\sim$700 Myr) for these low-mass (red) dwarf stars.

This explanation runs as follows: As discussed in the preceding section, we expect fully convective stars to be dominated by coronal structures with relatively small spatial scales, an expectation which is consistent with our modeling of the observed coronal X-ray emission by *ROSAT*. The consequence of this spatial behavior is most easily understood in terms of potential (i.e., current-free) models for the coronal fields. That is, if the surface fields are dominated by fields whose multipole expansion has little power at low orders (so that the dipolar and quadrupolar components are weak or absent), then the falloff of magnetic field strength from the stellar surface will be rapid (relative to the dipolar or quadrupolar cases), and hence the Alfvén point for winds from these low-mass stars will be relatively close to the stellar surface. Therefore, the effective "lever arm" for despinning as the star loses mass is also relatively small. That is, because the geometric dimensions of the field structures are small scale, their multipole expansion has most of its power at large wavenumbers, and thus their field strength decreases more rapidly with radius than for stars whose coronal structure is dominated by dipolar or quadrupolar geometry. While it is the case that our results constrain directly only the closed magnetic field structures, whereas the mass and angular momentum loss is the result of flows from "open" coronal regions (which are also not current-free, i.e., not potential), it remains true that the "open" structures associated with the X-ray-emitting structures we study here, viz., the stellar equivalent of solar "helmet streamers" lying above active region loop arcades, will have comparable dimensions to the surrounding closed structures. Hence, despite the fact that the total magnetic flux on these active stars may be relative large, it is the high-frequency spatial structure that leads to magnetic torques that are not very efficient in braking the rotation of low-mass dwarfs. By contrast, our results for the active G0 V star π^1 UMa suggest that at least its high-temperature component is relatively extended (§ 4.1). The more extended and apparently more "stable" corona of active G dwarfs, in contrast to that of the dMe flare stars, may be at the root of why these earlier dwarfs spin down more rapidly than the low-mass, red dwarfs.

The preceding qualitative discussion can be made quantitative by considering, for the sake of concrete illustration, the following very simple evolutionary model for the low-mass main-sequence population: Denote the number of dwarf stars at a given mass and time by $N(M, t)$; the number of emission-line stars (viz., dMe stars) by $N_{\rm dMe}(M, t)$, and the number of nonemission line stars by $N_{\rm dM}(M, t)$. These three quantities obey the obvious relation

$$N(M, t) = N_{\rm dMe}(M, t) + N_{\rm dM}(M, t) . \tag{8}$$

Now we shall adopt the following simplifying assumptions.

1. The mean birth rate of stars is a constant, i.e.,

$$\frac{d}{dt} N(M, t) = c_b(M) , \tag{9}$$

where $c_b(M)$ is the (constant) birthrate of stars of mass M. Note that one can (in principal) constrain $c_b(M)$ observationally because the total number of stars of mass M, $N_T(M)$, is just given by

$$N_T(M) = \int_0^{t_{\rm now}} c_b(M) dt = c_b(M) t_{\rm now} \tag{10}$$

and is, in principle observable.

2. The mean rate at which the number of emission-line stars changes is given by a balance between the birthrate of stars of that mass, and the rate at which these stars despin to become nonemission-line stars,

$$\frac{d}{dt} N_{\rm dMe}(M) = c_b(M) - c_d N_{\rm dMe}(M) ; \tag{11}$$

thus, we assume that emission-line stars represent the young phase of stellar activity evolution.

3. Finally, we assume that the rate of change of nonemission-line stars equals the rate at which emission-line stars spin down:

$$\frac{d}{dt} N_{\rm dM}(M) = c_d(M) N_{\rm dMe}(M) . \tag{12}$$

Note here that we allow the spindown rate c_d to be a function of stellar mass.

Based on this very simple model, one can now construct the variation of (for example) the observable ratios $N_{\rm dMe}/N_{\rm dM}$ and $N_{\rm dMe}/N_{\rm tot}$ with the spindown rate c_d; the result is shown in Figure 4, for an assumed average stellar birthrate of 10 yr^{-1} (and $t_{\rm now} \sim 10^{10}$ yr). This allows us to deduce the spindown timescale for a given class of stars by measuring these two ratios for volume-limited stellar samples; for example, from Figure 4, we see that the spindown timescale for stars in the mass range in which virtually all stars show strong emission lines must be very long (typically, $>10^{11}$ yr). We further note here that a similar analysis can be made using alternative activity indicators, such as the luminosity ratio $L_X/L_{\rm bol}$ (see Paper II).

This quantitative picture can be pursued somewhat further by adopting a specific model for the spindown mechanism. Consider, for example, the Weber & Davis (1967) model, for which the spindown timescale τ_d is given by the expression

$$\tau_d = c_d^{-1} \approx \frac{J}{\dot{J}} = \frac{3}{2} \frac{I}{r_A^2 \dot{M}} = \frac{3}{2} k \frac{M}{\dot{M}} \left(\frac{R}{r_a}\right)^2 , \tag{13}$$

where J is the stellar angular momentum, r_A is the Alfvén

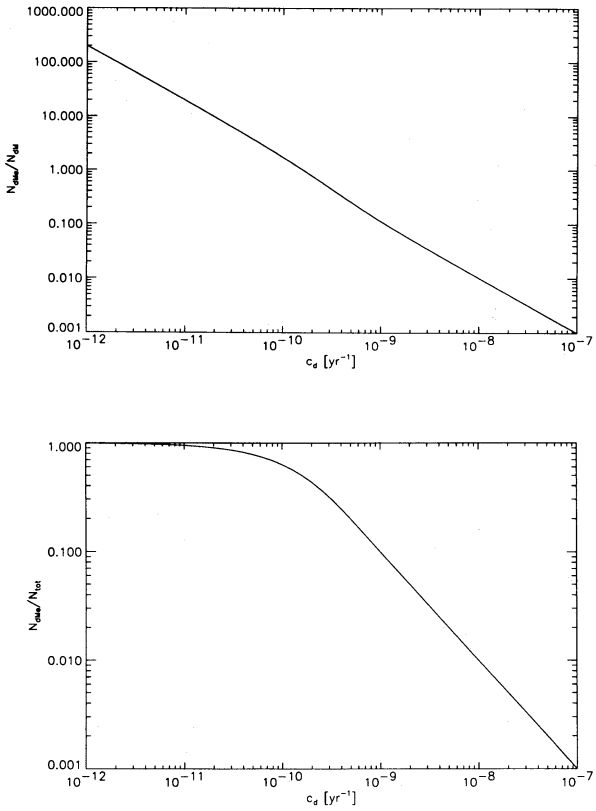

FIG. 4.—Comparison of the total number of dMe stars vs. dM stars (*upper panel*) and vs. all dwarf M stars (*lower panel*) at present, plotted as a function of the spindown rate for dMe stars; we assume a mean stellar birth rate of 10 yr^{-1}, for the simple stellar activity evolution model encapsulated in eqs. (8)–(12).

radius, and we have assumed that the moment of inertia for the star is given by $I = kMR^2$; M and R are the stellar mass and radius, respectively, and k is a adjustable parameter which accounts for our ignorance of the internal state of rotation of the stars in question ($k = \frac{2}{5}$ corresponds to solid-body rotation of a uniform sphere and is only weakly dependent on stellar density stratification for stars on the main sequence). This last equation encapsulates our earlier argument that the despinning timescale is a sensitive function of the lever arm for despinning (e.g., of the ratio r_A/R); indeed, this sensitivity is larger than is apparent from the explicit dependence of τ_d on r_A/R because the mass-loss rate $\dot{M}$ is itself dependent on the dynamo process, and hence on r_A/R; that is, as r_A decreases, so will $\dot{M}$ (although the precise nature of the decrease cannot be determined from our considerations), therefore enhancing the consequent increase in τ_d.

Furthermore, we can ask whether plausible estimates for mass-loss rates are consistent with our model. As an illustration, consider the mass-loss rate estimate (for flare-related losses) provided by Coleman & Worden (1977) of $\sim 2 \times 10^{-13}\ M_\odot\ \mathrm{yr}^{-1}$; then for $M/M_\odot \sim 0.3$, and $r_A/R \approx 2$, we find that $\tau_d \approx 10^{12}$ yr, or $c_d \sim 10^{12}\ \mathrm{yr}^{-1}$. That is, we would expect (on the basis of Fig. 4) that for such stars, the ratio of emission-line stars to all stars of that mass to be order 1. This is indeed observed.

We thank A. Maggio and G. Peres for useful comments. We acknowledge support by NASA grants to the NOAO (M. S. G.) and to the University of Chicago (V. K. and R. R.). This research has made use of the SIMBAD database, operated at CDS, Strasbourg, France.

APPENDIX A

PARAMETERIZATION OF POWER EMITTED BY RS THERMAL SPECTRUM WITH TEMPERATURE AND ABUNDANCE

Spectral fits of our program stars show that these stars may be significantly metal-deficient. In order to properly account for this deficiency in the coronal loop model, we devised a parameterization of the power emitted by optically thin thermal

TABLE 5

COEFFICIENTS OF $P'(T)$

Range of $\log_{10}(T)$ (K)	a (ergs cm^3 s^{-1})	b
[4.90, 5.00).....	4.3×10^{-21}	1
[5.00, 5.10).....	4.3×10^{-22}	0
[5.10, 5.30).....	9.7×10^{-22}	0.4
[5.30, 5.41).....	4.1×10^{-22}	−0.13
[5.41, 5.61).....	1.2×10^{-23}	−2.7
[5.61, 5.86).....	7.4×10^{-23}	−0.7
[5.86, 6.04).....	1.0×10^{-22}	0.2
[6.04, 6.23).....	1.0×10^{-22}	−0.16
[6.23, 6.59).....	2.2×10^{-22}	−1.5
[6.59, 6.77).....	3.3×10^{-23}	−0.12
[6.77, 6.83).....	9.7×10^{-24}	0.6
[6.83, 6.97).....	1.1×10^{-22}	−0.66
[6.97, 7.24).....	1.4×10^{-21}	−1.8
[7.24, 7.56).....	1.3×10^{-22}	−1
[7.56, 7.60).....	8.4×10^{-27}	1.7
[7.60, 8.00).....	5.2×10^{-24}	−0.05

plasma (Raymond & Smith 1977; Raymond 1988):

$$P(T, Z) = P(T, Z = 0) + ZP'(T) \text{ ergs cm}^3 \text{ s}^{-1} , \quad \text{(A1)}$$

where

$$P(T, 0) = 2 \times 10^{-27}\sqrt{T} + 5 \times 10^{-25}e^{\sqrt{2.8 \times 10^6 K/T}} + 3 \times 10^{-25} Y(T_L, T_H) \text{ ergs cm}^3 \text{ s}^{-1} , \quad \text{(A2)}$$

is the power emitted by a plasma with no metals, $Y(T_L, T_H) = 1$ for $T_L = 9 \times 10^5$ K $\leq T < T_H = 1.85 \times 10^6$ K and 0 elsewhere, and

$$P'(T) = aT_6^b ,$$

where $T_6 = T/10^6$ K, and the coefficients a and b take on the values shown in Table 5.

REFERENCES

Ambruster, C. W., Sciortino, S., & Golub, L. 1987, ApJS, 65, 273
Bessell, M. S. 1990, A&AS, 83, 357
Boeshaar, P. C. 1976, Ph.D. thesis, Ohio State Univ.
Butler, C. J., Rodonò, M., Foing, B. H., & Haisch, B. M. 1986, Nature, 321, 679
Coleman, G. D., & Worden, S. P. 1977, ApJ, 218, 792
Collura, A., Pasquini, L., & Schmitt, J. H. M. M. 1988, A&A, 205, 197
Cram, L. E. 1982, ApJ, 253, 768
Doyle, J. G., & Butler, C. J. 1985, Nature, 313, 378
Drake, J. J., Laming, J. M., & Widing, K. G. 1995a, ApJ, 443, 393
———. 1995b, ApJ, submitted
Drake, J. J., Laming, J. M., Widing, K. G., Schmitt, J. H. M. M., Haisch, B., & Bowyer, S. 1995c, Science, in press
Durney, B. R., De Young, D. S., & Roxburgh, I. W. 1993, Sol. Phys., 145, 57
Fleming, T. A., Giampapa, M. S., Schmitt, J. H. M. M., & Bookbinder, J. A. 1993, ApJ, 410, 387
Fleming, T. A., Gioia, I. M., & Maccacaro, T. 1989, ApJ, 340, 1011
Fleming, T. A., Liebert, J., Gioia, I. M., & Maccacaro, T. 1988, ApJ, 331, 958
Fleming, T. A., Molendi, S., Maccacaro, T., & Wolter, A. 1995a, ApJS, 99, 44
Fleming, T. A., Schmitt, J. H. M. M., & Giampapa, M. S. 1995b, ApJ, 450, 401 (Paper II)
Giampapa, M. S., Golub, L., Peres, G., Serio, S., & Vaiana, G. S. 1985, ApJ, 289, 203
Giampapa, M. S., & Liebert, J. 1986, ApJ, 305, 784
Gliese, W., & Jahress, H. 1991, Third Catalogue of Nearby Stars (Heidelberg: Astr. Rechen-Inst.)
Golub, L. 1992, in Physics of Solar and Stellar Coronae: G. S. Vaiana Memorial Symposium, ed. J. L. Linsky & S. Serio (Dordrecht: Kluwer), 71
Golub, L., Krieger, A. S., Silk, J. K., Timothy, A. F., & Vaiana, G. S. 1974, ApJ, 189, L93
Golub, L., Maxson, C., Rosner, R., Serio, S., & Vaiana, G. S. 1980, ApJ, 238, 343
Güdel, M., & Guinan, E. F. 1995, in IAU Coll. 152, Astrophysics in the Extreme Ultraviolet, ed. B. M. Haisch & S. Bowyer (Cambridge: Cambridge Univ. Press), in press
Haisch, B. M., Schmitt, J. H. M. M., Rodonò, M., & Gibson, D. M. 1990, A&A, 230, 419
Hempelmann, A., Schmitt, J. H. M. M., Schultz, M., Rüdiger, G., & Stępień, K. 1995, A&A, in press
Henry, T. J., & McCarthy, D. W., Jr. 1993, AJ, 106, 773
Kashyap, V. 1995, in Proc. 15th Internat. Workshop on Maximum Entropy & Bayesian Methods, Santa Fe, NM, ed. K. Hanson & R. Silver (Dordrecht: Kluwer), in press
Kashyap, V., Rosner, R., Micela, G., Sciortino, S., Vaiana, G. S., & Harnden, F. R., Jr. 1992, ApJ, 391, 684
Kashyap, V., Rosner, R., Schramm, D., & Truran, J. 1994, ApJ, 431, L87
Kirkpatrick, J. D., Henry, T. J., & McCarthy, D. W., Jr. 1991, ApJS, 77, 417
Klimchuk, J. A., Lemen, J. R., Feldman, U., Tsuneta, S., & Uchida, Y. 1992, PASJ, 44, L181
Lacroute, P., & Valbousquet, A. 1971, in IAU Colloq. 7, Proper Motions, ed. W. J. Luyten (Minneapolis: University of Minnesota Press), 153
Linsky, J. L., Bornmann, P. L., Carpenter, K. G., Wing, R. F., Giampapa, M. S., Worden, S. P., & Hege, E. K. 1982, ApJ, 260, 670
Linsky, J. L., & Wood, B. E. 1994, ApJ, 430, 342
Maggio, A., & Peres, G. 1995, A&A, in press
Meneguzzi, M., Frisch, U., & Pouquet, A. 1981, Phys. Rev. Lett., 47, 1060
Meyer, J.-P. 1985, ApJS, 57, 173
Mullan, D. J. 1984, ApJ, 282, 603
Mullan, D. J., Stencel, R. E., & Backman, D. E. 1989, ApJ, 343, 400
Pallavicini, R., Golub, L., Rosner, R., Vaiana, G. S., Ayres, T., & Linsky, J. L. 1981, ApJ, , 248, 279
Pallavicini, R., Serio, S., & Vaiana, G. S. 1977, ApJ, 216, 108
Pallavicini, R., & Vaiana, G. S. 1980, Solar Phys., 67, 127
Parker, E. N. 1983, ApJ, 264, 642
———. 1984, ApJ, 280, 423
———. 1993, ApJ, 407, 342
Randich, S., Schmitt, J. H. M. M., Prosser, C. F., & Stauffer, J. R. 1995, A&A, submitted
Raymond, J. C. 1988, in Hot Thin Plasmas in Astrophysics, ed. R. Pallavicini (Dordrecht: Kluwer), 3
Raymond, J. C., & Smith, B. W. 1977, ApJS, 35, 419
Reid, N., & Gilmore, G. 1984, MNRAS, 206, 19
Rosner, R., et al. 1981, ApJ, 249, L5
Rosner, R., et al. 1995, ApJ, 442, L25
Rosner, R., Golub, L., Coppi, B., & Vaiana, G. S. 1978, ApJ, 222, 317
Rosner, R., Tucker, W., & Vaiana, G. S. 1978, ApJ, 220, 643 (RTV)
Rosner, R., & Vaiana, G. S. 1977, ApJ, 216, 141
———. 1980, in X-Ray Astronomy, ed. R. Giaconni & G. Setti (Dordrecht: Reidel), 129
Rosner, R., Golub, L., & Vaiana, G. S. 1985, ARA&A, 23, 413
Rosner, R., & Weiss, N. O. 1992, in The Solar Cycle, ed. K. L. Harvey (San Francisco: ASP), 511
Saar, S. H., & Linsky, J. L. 1985, ApJ, 299, L47
Schmitt, J. H. M. M. 1990, Adv. Space Res., 10(2), 115
———. 1994, in AIP Conf. Proc. 313, The Soft X-Ray Cosmos, *ROSAT* Science Symp., ed. E. M. Schlegel & R. Petre (New York: AIP), 24
Schmitt, J. H. M. M., Collura, A., Sciortino, S., Vaiana, G. S., Harnden, F. R., Jr., & Rosner, R. 1990, ApJ, 365, 704
Schmitt, J. H. M. M., Fleming, T. A., & Giampapa, M. S. 1995a, ApJ, 450, 392 (Paper I)
Schmitt, J. H. M. M., Drake, J. J., Stern, R. A., & Haisch, B. M. 1996, ApJ, 457, 882
Schmitt, J. H. M. M., Haisch, B. M., & Barwig, H. 1993, ApJ, 419, L81
Schmitt, J. H. M. M., & Rosso, C. 1988, A&A, 191, 99
Schmitt, J. H. M. M., Haisch, B. M., & Drake, J. J. 1994, Science, 265, 1420
Schmitt, J. H. M. M., Harnden, F. R., Jr., Peres, G., Rosner, R., & Serio, S. 1985, ApJ, 288, 751
Schmitt, J. H. M. M., & Snowden, S. L. 1990, ApJ, 361, 207
Schmitt, J. H. M. M., Stern, R. A., Drake, J. J., & Kürster, M. 1995b, ApJ, submitted
Schrijver, C. J., Lemen, J. R., & Mewe, R. 1989, ApJ, 341, 484
Serio, S., Peres, G., Vaiana, G. S., Golub, L., & Rosner, R. 1981, ApJ, 243, 288
Sheeley, N. R., Jr. 1981, in Solar Active Regions: A Monograph from Skylab Solar Workshop III, ed. F. Orrall (Boulder: Colorado Associated University Press), 17
Singh, K. P., Drake, S. A., & White, N. E. 1995, ApJ, 445, 840
Stauffer, J. R., Caillault, J.-P., Gagné, M., Prosser, C. F., & Hartmann, L. W. 1994, ApJS, 91, 625
Stauffer, J. R., & Hartmann, L. W. 1986, ApJS, 61, 531
———. 1987, ApJ, 318, 337
Stauffer, J. R., Liebert, J., & Giampapa, M. S. 1995, AJ, 109, 298
Stern, R. A., Antiochus, S. K., & Harnden, F. R., Jr. 1986, ApJ, 305, 417
Stern, R. A., Lemen, J. R., Schmitt, J. H. M. M., & Pye, J. P. 1995b, ApJ, 444, 45
Stern, R. A., Schmitt, J. H. M. M., & Kahabka, P. T. 1995a, ApJ, 448, 683
Swank, J. H., & Johnson, H. M. 1982, ApJ, 259, L67
Swank, J. H., White, N. E., Holt, S. S., & Becker, R. H. 1981, ApJ, 246, 208
Trümper, J. 1983, Adv. Space Res., 2, No. 4, 241
Tucker, W. H. 1973, ApJ, 186, 285
Vaiana, G. S., & Rosner, R. 1978, ARA&A, 16, 393
Vainshtein, S. I., & Kichatinov, L. L. 1986, J. Fluid Mech., 168, 73
Veeder, G. J. 1974, AJ, 79, 1056
Vesecky, J. F., Antiochus, S. K., & Underwood, J. H. 1979, ApJ, 233, 987
Walter, F. M. 1983, ApJ, 274, 794
Weber, E. J., & Davis, L., Jr. 1967, ApJ, 148, 217
Withbroe, G. L. 1978, in Proc. OSO8 Workshop (Boulder: University of Colorado Press)